CONF-9506250--3

SLAC–PUB–95–6961
October 1995

PHOTON DETECTORS*

J. Va'vra
Stanford Linear Accelerator Center, Stanford University,
Stanford, CA 94309, U.S.A.

ABSTRACT

This paper compares the photon detectors used to date in high energy physics and astrophysics experiments, with particular emphasis on design features, problems and mistakes. The paper also describes a new direction in the area of photon detection.

Invited talk presented at the International Workshop on RICH Detectors (RICH 95)
Uppsala, Sweden, June 12-16, 1995

* Work supported by the Royal Swedish Academy of Sciences through its Nobel Institute for Physics, and Department of Energy contract DE-AC03-765SF00515.

INTRODUCTION

J. Seguinot and T. Ypsilantis have recently described the theory and history of Ring Imaging Cherenkov (RICH) detectors [1, 2]. In this paper, I will expand on these excellent review papers, by covering the various photon detector designs in greater detail, and by including discussion of mistakes made, and detector problems encountered, along the way. However, I will not consider overall system geometries, radiators, optics, gas systems, etc. As a result, there will be no discussion of angular resolution or the value of N_0 achieved in the various experiments.

Photon detectors are among the most difficult devices used in physics experiments, because they must achieve high efficiency for photon transport and for the detection of single photo-electrons. For gaseous devices, this requires the correct choice of gas gain in order to prevent breakdown and wire aging, together with the use of low noise electronics having the maximum possible amplification. In addition, the detector must be constructed of materials which resist corrosion due to photosensitive materials such as TMAE, the detector enclosure must be tightly sealed in order to prevent oxygen leaks, etc.

The most critical step is the selection of the photocathode material. Typically, a choice must be made between a solid (CsI) or gaseous photocathode (TMAE, TEA). A conservative approach favors a gaseous photocathode, since it is continuously being replaced by flushing, and permits the photon detectors to be easily serviced (the air sensitive photocathode can be removed at any time). In addition, it can be argued that we now know how to handle TMAE, which, as is generally accepted, is the best photocathode material available as far as quantum efficiency is concerned (see Fig.1 and ref.3). However, it is a very fragile molecule, and therefore its use may result in relatively fast wire aging. A possible alternative is TEA, which, in the early days, was rejected because it requires expensive CaF_2 windows, which could be contaminated easily in the region of 8.3 eV and thus lose their UV transmission; there was also a suspicion that it had low quantum efficiency. Although the CaF_2 windows are still expensive to use, the contamination problem appears to be manageable, and the results of several tests presented in this paper remove the second concern by confirming the high quantum efficiency reported in ref. 1. The TEA molecule is also not as fragile as the TMAE molecule, so that its wire aging effects should be less severe. This would certainly be helped by conditions of very low wire gain, as allowed by the use of slow, low noise electronics. In addition, TEA is a good quencher, and TEA-based detectors can operate at room temperature, and can be made thin.

In the area of solid photocathodes, there is a considerable R&D effort to promote use of CsI. This is easy to apply to a surface, such a detector can be operated at room temperature and has a faster response with parallax-free image reconstruction. To date, there are several test results, some of them encouraging. In addition, the Hamamatsu Co. is selling photo-multipliers (PM) which make use of such a photocathode. Nevertheless, the present situation is somewhat similar to that in early days of the use of

TMAE, in the sense that some experiment employing CsI detectors will have to run successfully for several years before this concept is generally accepted.

Finally, just as we are on the point of claiming that the art of constructing and operating real gaseous photon detectors is well-understood after many years of trial and error, we find that there are many physicists who will not consider the use of such complicated instruments. Rather, they encourage the use of devices which are as simple as possible, and which are based on commercially available photo-multipliers (PM's). Recently, the arsenal of such PM's has been augmented by the addition of hybrid PM's, multi-anode PM's, micro-sphere plate electron multipliers (MSP's), etc. This school of thought may very well prevail, since there have been recent encouraging R&D results with such devices. This would change the direction of the R&D work on photon detectors in our labs, much to the pleasure of the manufacturing companies. It is very possible that the next RICH workshop will see a very different photon detector menu than that reviewed in this paper.

1. SOME BASICS OF PHOTON COUNTING.

I have decided to cover three important topics relevant for the development of the gaseous photon detectors.

1.1. The determination of single electron efficiency.

Clearly, the best method of determining single electron efficiency is to plateau the efficiency using the photoelectrons on Cherenkov rings, and this has been done by several groups. However, this is applicable only in the final stages of an experiment. An alternative method, which can be used very early on, is to use the single electron pulse height spectrum fitted to a combination of a Polya and a Gaussian function. The spectrum should be obtained by using an external trigger on the pulse height analyzer; this yields a true noise spectrum together with the signal q. From the fit, the Polya function [4]

$$P(q) \approx \left[(1+\theta)\frac{q}{\bar{q}}\right]^{\theta} e^{-(1+\theta)(q/\bar{q})} \qquad (1)$$

is extracted, where the empirical constant θ is related to the first Townsend coefficient α through the equation : $\alpha(x,q) = \alpha(x)[1+(\theta/q)]$. The exact physical significance of the parameter θ is not clear. Nevertheless, equation (1) is widely accepted on the basis of empirical studies, and can be used to calculate the single electron efficiency ε for a known threshold, Th :

$$\varepsilon = \int_{Th}^{\infty} P(q)dq \Big/ \int_{0}^{\infty} P(q)dq. \qquad (2)$$

The fitted quantity $\bar{q}$ can be used to estimate the mean wire gain (see for example ref. 5). Fig. 2 shows an example of the author's analysis for the CRID detectors, including the calculated efficiencies. For a threshold of ~1.5x10^4 e$^-$, suitable for taking UV fiber data, the anode wire detection efficiency is ~95%. However, when running the hadronic trigger, which has higher background and larger cross-talk

problems, the threshold must be raised to ~2-3x10^4 e$^-$ in order that the total number of hits should fit into the system buffer; this causes the detection efficiency to decrease to ~85-90% (for the 1996 run, the buffer size will be increased in order to improve the efficiency). The point here is that the result of a successful bench test may be modified later due to complicated background and system considerations arising in the context of a real experiment.

Throughout the RICH literature, wire gain is specified in a rather inconsistent manner. In this paper, reference is made to two quantities : the "visible" gain, which refers to the charge integrated within the limited gate width of a particular test, and the "total" wire gain, which refers to the total charge developed after all positive ions have finished drifting (see Table 1 for examples).

1.2. The quantification of avalanche quenching.

As is apparent in Table 1, many experiments do not quote the secondary photoelectron feedback rate due to the gaseous or cathode processes initiated by avalanche photons. Those who quote this number actually make a cut on the minimum drift time before the secondary photoelectron is resolved from the primary avalanche (typically the cut is at 100-200 ns). However, when judging the long term stability of the detector, it is very important to take proper account of these secondary photo-electrons, especially for photosensitive detectors.

From empirical studies of gases with poorly quenched avalanches, Va'vra et.al. [5] have suggested using the single electron pulse height spectrum to judge the quenching behavior quantitatively. For a sufficiently long charge integrating gate, the secondary hits will tend to show up as an excess at large pulse heights, and the resulting spectrum will be characterized by a negative value of θ in the Polya function. This can be illustrated by means of a specific example from ref. 5 involving the CF_4 gas. Friese et.al. [6] have shown earlier that CF_4 gas emits photons at ~170 nm, which is right in the middle of the range of TMAE photosensitive acceptance. For this gas, a very clear example of avalanche breeding is shown in Fig. 3, which is taken from ref. 5. This effect can be stopped, and even reversed, by increasing the concentration of a good quencher; this is shown explicitly in Fig. 4, which shows how θ changes from negative to positive values with the addition of iC_4H_{10} [5].

The simple theory of the single electron multiplication process does not take into account secondary processes; it does not say anything about $\theta<0$. At small E/p, it predicts an exponential (Furry) distribution, corresponding to $\theta=0$ in equation (1), which is in good agreement with experiment. As E/p increases, either by increasing the gas gain (E) or by lowering the gas pressure (p), the Furry distribution typically changes to a Polya distribution with $\theta>0$ in equation (1). To predict such behavior, Raether [7], and subsequently Schlumbohm [8], suggested that the critical quantity to consider in the avalanche mechanism is a parameter, χ, which is the ratio of the energy gained between two subsequent electron collisions, eE/α, (α is the first Townsend coefficient, $1/\alpha$ is the mean free path, E is the electric field) and the ionization energy (eV_{ion}). For large values of χ(>25), the pulse height spectrum tends to be exponential ($\theta=0$), while for small $\chi<20$ it exhibits a Polya-type turnover ($\theta>0$). The theory was

subsequently expanded by Legler [9] and Alkhazov [10], among others. Experimental examples corroborating this theory can be found in ref. 11. For example, on the basis of results on TMAE-based gases from the DELPHI prototype (see Table 1), Arnold et.al. [12] report the following behavior of the θ parameter as a function of the visible gain G : $\theta=1.8\times10^{-6}$ G-0.095 for G>5.3×10^4 (i.e. $\theta>0$) and $\theta=0$ for G<5.3×10^4 (to get the total gain, multiply by a factor ~5). However, for detector designs where secondary processes play a significant role, the Furry distribution changes into a distribution with $\theta<0$ in equation (1) at large E/p values [5]. To my knowledge, nobody has suggested that a simple way of recognizing the presence of quenching problems is to look for values of $\theta<0$, as reported in ref. 5, although Raether has pointed out that, for large gain values, a pulse height distribution can fall faster than exponential (see page 81 in ref. 7), and Legler [9] has developed a more complex theory of avalanche breeding yielding similar empirical behavior.

However, reality can be even more complicated. In some special geometries, where the amplification gain may vary around the wire or across the amplification strip, this local response must be convoluted to obtain the final pulse height distribution. An excess of small pulses due to insufficient amplification around the wire may cause $\theta<0$ even without the presence of secondary processes. Nevertheless, in order to help evaluate a typical design, I quote the corresponding parameter θ in Table 1.

I would like to add one more comment. It is frequently argued that the pulse height distribution should have $\theta>0$ to ensure good single electron efficiency. Although this is generally true, good efficiency can be obtained even with a purely exponential distribution, provided that extremely low noise electronics performance can be achieved (see chapter 3.4). In hydrocarbon gases operating at normal pressure, the total gas gain must be increased typically beyond $3\text{-}5\times10^5$ in order to obtain good (i.e. $\theta>0$) behavior [5].

1.3. Charge collection in different geometries.

The induced charge on any electrode in a wire chamber is a complicated function of the electrostatic configuration, geometry, integration time of the amplifier, etc. [13]. I have decided to examine two extreme cases, one a typical MWPC chamber, and the other a micro-gap chamber [14]. Most of the detectors described in this paper belong to the first category. The important point is that a typical MWPC structure collects only ~20% of the total available charge in the first ~20 ns (see Fig. 5). This portion of gas gain is called visible gain in Table 1. Therefore, all detectors operating with very short charge integration times, say 10-100 ns, are using only a small fraction of the available charge, and tend to offset this by operating at large gain (total gas gain can typically reach $\sim5\times10^5$, in some instances $\sim10^6$). A small anode wire diameter, or a small anode-cathode distance, speeds up the charge collection, but the gain is only logarithmic. On the other hand, in a micro-gap chamber ~95% of the total charge is collected in the first ~20 ns , with an anode-cathode coupling ratio close to one [14]. However, the penalty for this performance is severe, since the surface field strength exceeds ~2.7 MV/cm.

For example, the MWPC detectors for long drift TPC's (DELPHI, SLD, OMEGA - see Table 1), need a short integration time (10-100 ns) in order to distinguish two nearby hits, although all of these detectors are actually considered to be slow devices because of the long drift times involved.

Another example is the FAST RICH MWPC chamber with cathode pad readout. For short integration times, the size of the induced charge on the cathode is considerably smaller than that at the anode; to compensate for the lower signal on the cathode, a very small anode-cathode spacing must be chosen, and the chamber must be operated at higher gas gain. This in turn increases the cathode surface gradients, which may be relevant for the CsI photocathode solutions. To cope with very high rates, very short integration times will be necessary at future hadronic colliders, such as LHC. Therefore, gaseous photon detector applications will be more difficult to implement. However, in many applications, such as the B-factory, the occupancy rate per pad is small, so that a very long integration time can be used. For example, the AMPLEX chip [15], as used by the RD-26 prototype, has integration time ~600 ns , and the VIKING chip [16], as used in the Cornell prototype, has integration time ~1 μsec (see Table 1). With such electronics, it is possible to operate with total gas gain below $\sim10^5$, since, for such long integration time constants, more charge is available, and the electronic noise is smaller.

Lowering the gas gain by a factor of five or more is very significant for the solution of many problems such as wire aging, sparking, wire breaking, cross-talk, photon feedback, etc. (see chapter 2). I believe that this is the right direction in which to develop new gaseous photon detectors, as will become even more clear in the next chapter.

2. EXAMPLES OF PHOTON DETECTOR PROBLEMS.

Many effects mentioned in this section are common to all gaseous detectors. However, photon detectors amplify the problems, because they require detection of a single electron, and operate with photosensitive materials, which tend to have complicated chemistry. The aim of this chapter is to convince the reader that it is very important to operate such detectors at low gas gain.

2.1. Wire aging (anode related effects).

This effect is caused by an accumulation of polymerization deposits on the anode wires. I will discuss mainly TMAE aging because, to my knowledge, nobody has tested TEA yet.

A high rate of polymerization is expected in TMAE-laden gases because the low mean ionization potential of the TMAE molecule (5.4 eV) provides the photoionization capability, and because the N-CH_3 bond strength is less than 3 eV, giving a high degree of fragility. The polymerization deposits are good insulators , and cause a drop in wire gain, with a subsequent loss of efficiency. A large gain drop was observed in early R&D tests [17, 18], and was subsequently confirmed in different test configurations [5, 19]. The early tests [17, 18] found a number of interesting dependencies : (a) the wire aging rate decreased with an increase in the complexity of the hydrocarbon molecule of the carrier gas; (b) it decreased with an increase in the diameter of the anode wire (see Fig. 6); (c) it did not seem to depend on TMAE concentration, gas flow, anode material, detector temperature, or source intensity; (d)

the anode wire deposits appeared to consist of a thin film which reacted with air to form droplets after the chamber was opened (these droplets could be easily washed away using alcohol, but if left on the wire, they would slowly increase in viscosity, and after a year would have the consistency of honey); (e) the anode wire aging deposits could be evaporated easily by passing a small current of about 10 mA through the 7 μm diameter carbon wire.

Anode wire aging is not so threatening if anode wire of larger diameter is used. A gain drop of 30-50% after a few mC/cm with a 33 μm diameter carbon wire (see Fig. 7) could be compensated for by adjusting the high voltage. In high rate applications, the use of carbon wires has some advantage because they can be cleaned periodically in situ by sending a small current through them [17].

To date, most large experiments have accumulated a negligible charge dose, and so are unable to confirm the test results directly. In fact, in most case, the wire aging is not yet a problem. However, the SLD CRID, which uses very thin 7 μm diameter anode wires, has observed a gain drop of about 15-20% in the first four years of operation, while accumulating a charge dose of about 0.01-0.1 mC/cm of wire length. Similarly, the OMEGA RICH [20] observed a very large gain drop in the 1991 run after a charge dose ~1 mC/cm (see Fig. 8); note that based on the test results [5] shown in Fig.6, a gain drop of ~60% would have been expected. The OMEGA RICH wire aging problem was subsequently solved by operating at somewhat lower gas gain, and by running with gating (the most significant effect), which reduces the charge accumulation rate by more than a factor of ten. Both results are consistent with the earlier R&D results [5, 17, 18].

2..2. Cathode related effects.

All photosensitive materials, and, very probably, their various aging deposits, are good insulators. In the presence of a large background, positive ions deposited on the cathode surface may cause a large increase in the electric field across such an insulating layer; this, in turn, may cause emission of electrons from the cathode, i.e. the well-known Malter effect [21]. What is not often realized is that the detector may operate in a mode where such currents are excited momentarily, but decay quickly in time. Such behavior is very difficult to observe, because the high voltage current trip is set higher than the magnitude of this effect. It took a great deal of detective work to discover such an effect in the SLD CRID detectors [18]. In fact it was not noticed until several 7 μm wires broke; these were presumably weakened by the local heating which occurs during such bursts. If a larger anode wire diameter had been chosen for the detector, it is probable that this effect would have gone unobserved. It was found that running UV fiber calibration data continuously over several years caused damage to cathodes corresponding to wire locations aligned with the UV fiber fiducials. The damage would show up as a burst of charge every 15-20 minutes. All bursts lasted longer than one Barrel CRID readout cycle, ~35 μsec, and less than ~0.5 sec, which corresponds to the nearest possible trigger, i.e. the burst is "self-extinguishing". The UV lamp trigger rate was 120 Hz, and resulted in a photoelectron effective rate of ~10/cm/s along the wire length in some locations (with the exception of SLC background electrons or

muons passing parallel to the TPC axis, this was typically the highest charge density per unit wire length). The 15-20 minute period corresponds to several time constants associated with charging of the film, where $RC = \varepsilon_r . \varepsilon_o . \rho_{film}$, $\varepsilon_r \sim 4$ and $\rho_{film} > 10^{15}\,\Omega$cm. For an average wire total gas gain ($\bar{G} \sim 3\times10^5$) and the 15-20 minute charging time, a charge density of more than 10^9 ions per few square mm of the cathode surface could be reached, and this would result in fields of more than 100 kV/cm across the insulator (if the film were sufficiently thin (<100 Å), the "static" behavior of the chamber would not be altered). Such values could exceed the dielectric strength of the film, and a breakthrough of electrons could occur. In addition, such fields begin to be significant for the Schottky reduction of the work function of the cathode metal , i.e. the cathode can become photo-sensitive. After the problem was discovered, the UV fiber trigger rate was reduced by a factor of 2000, and this yielded a reduction of the burst rate by more than a factor of 20.

In ref. 18 it was suggested that the addition of a small amount of water (~20ppm) would prevent charging effects in TMAE-based detectors which are not opened to air for several years. In addition, their gas systems have been designed to remove water in the first place, and vacuum pumping on TMAE during cleaning preferentially removes water. Water could be added to the gas during shutdown periods, if not during the TMAE run. It is necessary to add water to many drift chambers to prevent similar charging effects. This area needs to be investigated in more detail, but all our prototypes had at least this much water during all R&D testing with TMAE, and at this level no detrimental effect on the electron lifetime has been observed.

It is natural to ask if similar effects could exist in CsI-based chambers. Recently, the volume resistivity of the CsI film was measured [22], and its value found to be between 10^{11} and $10^{12}\,\Omega$cm. This gives a protection of 3-4 orders of magnitude, if the volume resistivity remains stable over many years of experiment. Not much is known about TEA in this respect.

2.3. Quenching and sparking.

A cathode next to anode wires can be coated either directly (CsI) or indirectly (TMAE, TEA, wire aging deposits of TMAE, etc.) by a photosensitive material. The avalanche photons can cause emission of secondary photoelectrons. If the efficiency of this process, η, and the total gas gain, G, are high enough that $\eta.G \sim 1$, the chamber goes into a self-sustaining current mode, and becomes very unstable. If η is small, such photoelectrons cause extra noise only, and this problem can be solved by a suitable choice of an electrode blind structure (see Figs. 5, 6). However, a better way to deal with this problem in future would be to choose : (a) lower gas gain, (b) a structure which allows only small primary charge deposits (a thin detector or low pressure operation), and (c) a suitable gas (for example iC_4H_{10}). The advantage of the TEA-based photocathode in this respect is a very short photon absorption length ($\ell_{abs} \sim 0.6$ mm), which limits the effect of avalanche photons and allows a thin detector structure. The quantitative procedure for evaluating quenching was outlined in chapter 1.2.

If the number of primary ion pairs, $N_{prim.ion.}$, and the total gas gain, G, are such that the condition $N_{prim.ion.}.G>10^8$ is satisfied, the chamber will spark. This is the well-known Raether condition [23], derived 40 years ago, and recently rediscovered in our field [24]. For example, a slow electron or a muon moving along the axis of a 1.2 m long TPC, as in the SLD barrel CRID, could deposit more than 10000 primary electrons. The Raether condition may be satisfied occasionally, especially if coupled with the discharges described in chapter 2.2. This may have caused the breakage of 7 μm diameter carbon wires [18].

2.4. Solid photocathodes.

Solid photocathodes, such as CsI, are not without possible problems either. Aging studies of the quantum efficiency are still in the very early stages, and we would recommend that their significance not be underestimated. Photocathode damage may occur : (a) by light exposure only (no gain), (b) by gas gain, (c) by sparking, (d) by environmental damage due to gas-related effects of all sorts, air exposure, temperature, etc., and (e) by an "electrolytic" current through the volume causing the plating of the ionic species on various electrodes. In my opinion, the last point is the most important. It is well known that the ionic species migrate under the influence of the potential in alkali halides [25]; Cs ions will migrate to the surface in a typical FAST RICH detector with pad structure, and similarly, Cs and I ions will migrate to cathode and anode respectively in micro-strip detectors operating in reflective mode. For example, only one week of running 100 Volts across the anode-cathode micro-strip structure covered by the CsI photocathode clearly showed plating deposits on the anode electrode, after it was subsequently exposed to air (the deposits are believed to be iodine) [22]. Similarly, aging under the influence of gas gain could be related to a migration of Cs ions to the photocathode surface, which subsequently reacts with either avalanche related ions, or gas system impurities, or air when the chamber is finally opened. This may explain the rather large difference in recent results, where a 20% quantum efficiency drop is claimed in one test after ~1 μC/mm^2 [26], in another after ~80 μC/mm^2 [27], and in a third after ~15 μC/mm^2 [28]. Clearly, more work is needed in this area.

3. EXAMPLES OF DETECTORS FOR CHERENKOV PHOTON IMAGING.

I have divided the existing photon gaseous detectors into groups according to the time response of the detector itself, the speed of the electronics, and special features such as geometry or gas pressure. The design and the basic operating parameters of the gaseous detectors are summarized in Table 1.

3.1. RICH using "LONG" drift.

I include in this group the photon detectors used by the DELPHI prototype [29], UA2-RICH [30], DELPHI barrel and endcap [31, 32], SLD CRID barrel and endcap [33, 34], OMEGA [35], and RICH-I [36]. All detectors in this group have demonstrated that they can do physics, handle the complicated chemistry of the TMAE photocathode, and survive a five-year-long experiment. This is a highly non-trivial accomplishment.

The photon detectors in this category are shown schematically in Figs. 9 and 10. It should be noted that a different approach has been taken to solving the detector geometry in endcap detectors (Fig. 10), where E is perpendicular to B. For example, the SLD Endcap CRID [34] chose a slow CO_2/C_2H_6-based gas mixture to reduce the electron drift velocity in order to minimize the Lorentz angle.

In all devices in this group it is necessary to resolve photoelectrons a few mm apart, which means that the electronics must have fast shaping time (10-100 ns). As a consequence, only a small fraction of the total charge developed on the anode wire is detected (see chapter 1.3.), which requires operation at a moderately high value of total gas gain (~3-6x10^5). Moreover, amplifier noise is usually not optimum for such short shaping times, and this, in turn, means even higher gas gain operation. This increases the rate at which avalanche photons either enter the drift volume or strike the neighboring electrode surfaces, where they can generate secondary photoelectrons. In the early days of Cherenkov Ring Imaging TMAE-based detectors, it was decided to "baffle" each anode wire using an electrode "blind" (see Figs. 9 and 10). As discussed in chapter 2, this helps the off-line analysis by simplifying the event, but it does not help chamber avalanche quenching issues. Another effect to be dealt with is the baseline shift which occurs after a large dE/dx charge deposit [33]; this problem can be solved by using a logarithmic response amplifier [32]. A better way to deal with both the above problems is to lower the gain and to decrease the thickness of the active part of the detector. However, in the 1980's, nobody would have dared suggest trading high gain operation, fast shaping time and long drift, for a full pixelization of a ~15 m^2 area and slow response, in order to operate much simpler detectors at low gas gain and higher temperature.

A common feature of all these devices is a long drift time (tens of μsec), and therefore a susceptibility to possible space charge effects which can cause rate-dependent drift distortions [33]. To my knowledge, none of the large experiments has reported any such distortions so far. Only the OMEGA RICH is using gating, mainly to reduce wire aging. The SLD CRID detectors [33, 34] deserve special comment because they are using charge division on 7 μm diameter carbon wires to measure the coordinate across the depth of the TPC. This technique has some advantages, namely a smaller number of electronics channels, and a larger anode-cathode distance, since the cathode is not read out; furthermore, the detector is more simple mechanically because the cathode is one simple block, resistive wires (~40 kΩ) behave very well electrically, and, in addition, they can be used to remove wire aging deposits when heated by passing a small current [18]. However, the charge division resolution required places a limit on minimum gas gain (σ_ℓ/ℓ~2.5% achieved at a total gas gain ~3x10^5), and the five-year-long experience has demonstrated that thin carbon wires are simply too fragile for such a large experiment (the breaking rate is one every few months on average in a system of ~5000 wires). The wire-breaking theory was outlined in chapters 2.2 and 2.3. Perhaps, in future, carbon wire of diameter in the range of 15-25 μm could be considered.

For future applications, the following features of the devices in this group should be avoided (see Table 1) : (a) relatively large electronics noise, especially in ref. 29, 31 and 36, (b) large total gas gain, especially ref. 29 and 35, (c) extremely thin anode wires [33, 34], (d) large active thickness; this causes traversing charged particles to generate large dE/dx deposits, which result in a large photon feedback rate, cross-talk, aging, etc.

3.2. RICH using "SHORT" drift.

I will mention only one device : the Fast Drift CRID prototype ([37] and Fig. 11). This was proposed in order to limit the drift time to a few μsec. Photon feedback is controlled by allowing only a small dE/dx deposit per traversing track (a 5 mm thick segment), and by making a suitable choice of gas and gain [5]. This is done by orienting the wires perpendicular to the traversing particles, by running the TMAE bubbler at a temperature of 40°C, and by using quartz-only construction to avoid thermal effects. To avoid wire breaking, thicker carbon wires (33 μm) is used. To resolve multiple hits, it is necessary to use a relatively fast shaping time (~ 65 ns), which means higher gas gain operation. The carbon wire is used to measure charge division along its length, and this also puts a lower limit on the gas gain. This classifies this particular detector in the group of higher gain devices, along with the detectors from chapter 3.1. In view of the arguments presented previously, this is an important disadvantage.

So far, the average value of the maximum total gas gain of the prototype has been limited to ~6-8x10^4 in C_2H_6+TMAE (40°C) gas, which is ~10 times lower than in the CRID detectors [33]. This has resulted in a pulse height spectrum with θ=0. The amplifier noise was also larger (~2500 electrons rms) due to the smaller resistivity of the thicker carbon wire [33]. Insufficient gas gain may result from the use of anode wire which is too thick, given the small anode-cathode gap of only 0.8 mm (gain variation around the wire is perhaps related to this). Clearly, the device needs at least one more iteration using anode wire of smaller diameter (~17 μm).

3.3. RICH using a "FAST" MWPC with "FAST" electronics.

In this group I consider CERES [38] (see Fig. 12), the College de France "TEA" and "CsI" prototypes [39, 40] (see Fig. 13) and the HERA-B "CsI" prototype [41]. These devices are designed for high rate applications, therefore they use small anode wire spacing, small anode-cathode gap, and the shortest possible detector integration times (10-20 ns).

For example, the College de France TEA-based prototype [39] used a total gas gain of about ~4x10^5, which was necessary given the requirement of high detection efficiency of the cathode pad readout (see Table 1). When the chamber was operating with a TEA-based gas mixture, this gain was sustained during the prototype test [39]. However, when the same geometry was used with a CsI photocathode [40], the prototype achieved a gas gain ~5 times smaller, which led to a small cathode pad efficiency. The gain limitation was observed in the test beam at high particle flux, which triggered discharges. It is very likely that the problem is related to the very small anode-cathode distance in this particular design (~0.5 mm), which causes rather high cathode surface field (8-10 kV/cm). Unfortunately, this prototype

had only digital electronics, and therefore no information about the pulse height spectra was obtained. Indirectly, the results are consistent with θ=0. In addition, a systematic degradation of the CsI quantum efficiency was observed in a separate test chamber designed to study the effect of pollution from the G-10 boards (a factor of 2 loss at 160 nm, and a factor of 6.5 at 200 nm over a period of only 75 days) [40]. The HERA-B "CsI" prototype [41] achieved only ~75% detection efficiency with θ<0.

The CERES TMAE-based detector [38] solved the problem by distributing the total gas gain over three stages, namely two parallel amplification gaps and one MWPC anode wire plane. When the detector operated with three parallel plate stages, it experienced severe sparking problems in a high background environment. Obviously the detector was reaching the Raether sparking condition, $N_{prim.ion.}.G > 10^8$. The solution was to replace the third amplification stage with the MWPC stage. The nonlinearity of the wire amplification limits the total gas gain, so that Raether's condition is not satisfied. No wire aging has been observed for the CERES detector so far (with ~20% uncertainty). It is possible that reducing the avalanche charge density in three-stage amplification with a highly diffusive He-based gas mixture is a clue to a possible solution to the problem of TMAE aging. This may be consistent with the TMAE test results indicating that a larger anode wire size causes a smaller wire aging rate [5, 17, 18], and that a parallel plate chamber has a smaller aging rate than a MWPC structure [19]. The CERES detector has achieved its N_o and resolution design goals, and the collaboration publishes physics papers.

3.4. RICH using a "FAST" MWPC with "SLOW" electronics.

Here I mention the prototype work of the RD26 collaboration, which includes the detectors developed by CERN [42], Saclay [43], and Munich [44] for the ALICE and HADES experiments, the Princeton prototype [45], the Cornell "TEA" prototype [46], and the detectors intended for the balloon experiments CAPRICE [47] and RICH-II [48]. All these devices use a cathode pad structure to detect single electrons, and have a geometry similar to that of the "CsI" prototype in Fig. 13 (see Table 1 for variations). To solve the gain dilemma of the previous chapter, the detectors in this group use much slower electronics to integrate the detector charge over 400-600 ns, together with relaxed geometrical distances. The long shaping time is possible because high single pad occupancy is not expected in these experiments.

For example, the RD26 CERN prototype [42] uses a 2 mm anode-cathode gap and 4 mm anode wire spacing, with an average value of total gas gain ~6-8x10^4. The detection efficiency is somewhat low (~85-90%), due to a combination of somewhat larger noise rate (~1500-2000 e^- rms) and θ=0 (Fig. 14a). As the gas gain increases, the θ parameter becomes slightly negative, indicating the possible onset of secondary processes (Fig. 14b). Similar signs of a quenching problem exist in the HADES prototype as the operating voltage is increased [44]. Perhaps, more work is needed to reduce amplifier noise in these devices. The Princeton prototype [45], on the other hand, uses a much larger anode-cathode spacing, which probably helps to achieve higher gain with well quenched pulse height spectra which have θ>0 (Fig. 14c). The detection efficiency is higher than 97% at 4100 V. The onset of possible

secondary effects can be seen above ~4100 V. However, one consequence of the larger anode-cathode gap is a larger spread of the cathode induced charge, i.e. the ring images are less clear, and have an increased probability of overlap.

The recent Cornell prototype [46] represents a nice advance. It uses very slow electronics (integration time ~1 μsec) with very low noise (~400 e^- rms). As a result, a high detection efficiency (~97%) is achieved, even with low total gas gain (~3-4x10^4) operation, which results in θ=0. The TEA-based photocathode gives sufficiently high quantum efficiency that ~13 photo-electrons per image are observed at θ_{dip}=30° with a 1 cm thick LiF radiator (~30% higher than in ref. 39). The difference could easily be due to transparency losses in the CaF_2 window caused by either an epoxy outgassing, or by mistakes during the evaporation of the conductive strips. Such a contamination is a problem in TEA-based detectors, since it is very easy to absorb 8.3 eV photons.

The CAPRICE detector [47] demonstrated that a TMAE-based system can be operated successfully even in a balloon flight, at high detector temperature (~50°C) and without electrode blinds, provided that the detector is made thin in order to limit dE/dx charge deposits. It uses the AMPLEX electronics [15] with an integration time 400-600 ns, visible gain ~10^5, which results in θ>0 and the anode detection efficiency >90%. Because of technical reasons specific to this particular balloon flight the cathode detection efficiency is only ~60%; this will be corrected in future flights, and the detector will have an efficiency similar to the RD26 CERN prototype [42], i.e. 85-90%. RICH-II [48] is, to a large extent, a similar detector. The reason it replaced RICH-I [36] was to allow operation in a stray magnetic field in future flights. All balloon experiments are now turning to ring detection of Z=1 particles since CAPRICE has shown that it is feasible. These experiments have one nice additional feature; they are finished after the 10-20 hours of a typical balloon flight...

3.5. RICH with "SPECIAL CONDITIONS".

3.5.1. RICH with "SPECIAL" geometry.

I want to mention the JETSET [49] (Fig. 15a), the HERA-B "TMAE" [50] and the new College de France "TMAE" [51] (Fig. 15b) prototypes. The main attraction here is that these designs allow operation at ambient temperature with good suppression of photon feedback. The JETSET detector uses individual cells made of reflective aluminum. To prevent amplifier saturation, the design uses logarithmic response. To minimize photon absorption, a quartz plate was drilled, and the anode wires are supported in the resulting holes. The HERA-B "TMAE" prototype uses an internal wire support structure, which results in an additional ~15% loss of photons, and cell walls made of bronze.
T. Ypsilantis presented a new "TMAE" conversion of their previous "TEA/CsI" prototype [51], combining the idea of the JETSET detector blind structure and the already existing MWPC pad structure [39, 40]. However, the cell walls are made differently : they use a G-10 material painted with lacquer for smoothness, then plated with silicon and MgF_2 films to maximize photon reflectivity, and equipped with conducting strips to grade the electric field. The blind structure is separated from the MWPC structure

by a mesh, which will reduce possible charging problems. The detector will be equipped at some point with slow electronics to be able to reduce the gas gain. It could be used in medium-rate applications.

The JETSET detector is an interesting idea for some applications. However, the original detector must have some efficiency losses due to gas gain variation near the quartz wire support. The aluminum surface is also not particularly reflecting to UV photons. The HERA-B prototype has an additional ~15% "photon loss" due to the wire support behind the quartz. The College de France solution [51] removes both of these problems at the expense of higher complexity. In the absence of gating, TMAE aging would be a concern.

3.5.2. RICH with "LOW" pressure operation.

I want to mention here the HELIOS "TMAE" pad[52] and PHENIX [53] prototypes. The former was a prototype for the CERES detector [38], which chose a helium-based gas mixture operating at 1 atm instead, because of technical difficulties connected with supporting a large window at low pressure. However, it should be noted that the low pressure detector [52] worked well; Figs. 16a,b compare their single electron pulse height spectra. Generally speaking, low pressure detectors, especially those with parallel plate structures, can reach very high gas gain, and have a very nice Polya pulse height spectrum with θ>0 [54, 55]. This observation can be explained using two arguments : (a) see discussion about the Polya shape dependence on the pressure in chapter 1.2, and (b) the double or triple parallel plate amplification suppresses the rate of secondary photoelectrons; in a single parallel plate gap, a secondary photoelectron will be fully amplified only if it crosses the gap completely. This is not the case in a MWPC structure. Single gap MWPC detectors, although more resistant to sparking due to their amplification nonlinearity, are more sensitive to secondary photo-electrons. To illustrate this point, Fig. 16c shows the single electron pulse height spectrum obtained from the low pressure, two-stage parallel amplification gap detector, operating with a fast amplifier, and an average total gas gain ~7x10^6 in 20% Ar+80% C_2H_6 gas at 10.3 Torr [56]. The Polya fit gives θ=+0.4, and indicates no sign of secondary processes even at such a high gas gain. This would not be possible to achieve with a single gap MWPC detector operating at normal pressure.

3.5.3. RICH with "OPTICAL" readout operation.

The HELIOS [57] (see Fig. 17) and NA35 [58] TMAE-based prototypes represent devices where CCD-based optical imaging is used instead of the usual wire or cathode pad electronics. There is an obvious attraction in their simplicity. So far, they have used TMAE-based gases. TMAE emits visible light of about ~400 nm wavelength during avalanche excitations, and this is a good match to the typical wavelength acceptance of a CCD. However, the overall optical efficiency of these system is still too low; this forces the chamber to operate at too large gas gain (~10^7), thus approaching Raether's sparking limit; a deposit of only 10-20 primary electrons will cause a spark. In the case of the NA35 beam test, there was at least one spark every spill. This is not tolerable for any physics operation. In order to make

progress in this area, more work is needed along the lines of new light-producing gases, more efficient optical systems and new resistive meshes (limiting spark formation).

3.6. RICH using "MICRO-STRIP" and "MICRO-GAP" gas chambers .

I will mention here the Munich micro-strip [59], the INFN Pisa micro-gap[60] and the Weizmann low pressure micro-strip [61] prototypes; Fig. 18 shows their geometry. Detectors of this type are known to reach only relatively small gas gain before surface breakdowns occur. One way out of this problem is to use a slow amplifier with extremely good noise performance, for example, the one used in the Cornell prototype [46]. However, this would eliminate the possibility of high rate operation of these devices (see chapter 1.3). Another approach is to use a double amplification scheme, where the first gain is obtained from the usual biasing of the surface electrodes of the micro-strip or micro-gap surface, and the second gain is obtained from the appropriate biasing of the main anode-cathode gap; Fig. 19 shows an example of the micro-gap pulse height spectra [60]. Clearly, the spectrum can be affected by the details of the chosen electrostatics. Although the achieved total gas gain in the INFN prototype [60] is impressive (2-3x10^5), its possible fragility requires more study before a large scale photon detection application is possible. The same is true for two micro-strip attempts [59, 61]; Fig. 20a shows the pulse height spectrum in the Weizmann micro-strip prototype, indicating $\theta<0$. The result may indicate that a more complicated avalanche mechanism is occurring when mixing the strip and the gap amplifications (see chapter 1.2). Some avalanches may proceed with small gain, resulting in an excess of small pulses.

3.7. RICH using photomultipliers.

The DIRC detector [62] is a novel concept proposed by B. Ratcliff. It has been chosen recently for the B-factory experiment at SLAC; Fig. 21 shows the principle. Cherenkov radiation is created in the quartz bar of rectangular cross-section. The detector uses a portion of the Cherenkov light which is internally reflected in quartz, and is normally lost in CRID/RICH designs. The ring image is preserved as the light propagates to the end of the bar, and emerges through the water-filled standoff box into the phototubes. It works in the visible wavelength region (in fact, quartz attenuates too much in the UV region, i.e. the imaging using TMAE-based detectors is not possible). The actual imaging is done in the phototubes (~15000 one inch diameter Hamamatsu tube R268). Recent encouraging beam tests have established that the concept is feasible. In principle, the DIRC has a superior yield of photoelectrons (2.7-5 σ π/K separation is predicted at 3.5 GeV/c, depending on the dip angle), and it has a very fast time response (< 1 ns resolution is possible). However, a number of technical questions remain, since nobody has built such a large, high quality optical system in any high energy experiment to date. For example, the required quality of the ~4 m long quartz bars is considerable (~0.25 mrad squareness, high quality sharp edges (< 5 μm in radius), high reflectivity of the polished surfaces (~99.995%), and >10 m attenuation length in the visible spectrum), and this raises issues concerning their handling, the possible degradation of reflectivity due to pollution of the surfaces, quartz bulk imperfections, distortions, etc.; there is also

the issue of the long-term purity of the water in the stand-off box. Cherenkov ring imaging with photomultipliers has been done successfully before in a Fermilab experiment E781 [63].

3.8. RICH using multi-anode PM, hybrid PM and MSP detectors.

Here I mention three examples : multi-anode PM's [64, 65], hybrid PM's [66, 67, 68] and MSP's [69]. The pioneering work on the multi-anode PM concept can be found in ref. 64. Recently, Hamamatsu introduced a similar commercial tube, the R5900-01-16L [65]. One possible way to simplify the DIRC with the water tank and ~15000 phototubes is shown in Fig. 22 [70]. The water tank is replaced by a large piece of quartz plate. The Cherenkov angle binning is done in two orthogonal dimensions, one dimension using narrow quartz bars, and the other the multi-anode PM [65]. These tubes have very good timing resolution (transit time spread σ~70 ps) and good single electron pulse height spectra.

Hybrid PM's have silicon pin diodes built into the PM structure, as can be seen in Fig. 23a [66]. The electronics is placed outside the tube, and a superb pulse height distribution is obtained (Fig. 23b). Such structures have modest gain (~3500), and require an additional amplifier and relatively high voltage operation (~15 kV); they exhibit negligible dark current and acceptable aging rate (a factor of two after a charge ~10 C). The disadvantage of such a concept lies in the limited number of channels that can be brought through the vacuum enclosure. Very recently, this problem was solved by placing a micro-diode detector together with its readout electronics into the vacuum tube (see Fig. 24) [67]. This was a brave step, considering the difficulties of producing good quality visible photocathodes. T. Ypsilantis reported on another LHC related development of a 256 diode element hybrid PM [68]. Each pixel is 5x5 mm, and the array will have an amplifier inside each vacuum enclosure. It will have a photocathode for visible light, and has been proposed for the LHC-B experiment [71].

Finally, the micro-sphere plate electron multiplier (MSP) [69] is a structure created by sintering small micro-balls which act as electron multiplication surfaces (see Fig. 25). The advantages of this concept are high gain (~10^7), well-behaved pulse height spectra, low voltage operation, and reasonable aging rate (~30 mC/cm^2). This structure has yet to be combined with a visible photocathode, although the attempts to combine it with a CsI photocathode are in progress. Also, its rate capability, dark current and uniformity of response are yet to be studied.

4. TMAE, TEA or CsI-BASED PHOTOCATHODE ?

Some issues have been already considered above. I would like to add here only a discussion of N_o (clearly, to discuss the angular resolution requires knowledge of the overall geometry). I consider four geometries relevant for a B-factory experiment such as BaBar, in this comparison : (a) the CAPRICE TMAE-based detector [47], suitable for the endcap region, (b) the Fast Drift CRID TMAE-based design [37], suitable for the barrel region, (c) the Cornell TEA-based design [39, 46], and (d) the RD26 CERN CsI-based design [42]. The TEA-based design has a LiF radiator, and the CsI-based design has only one window separating the C_6F_{14} liquid and the photocathode (the TMAE-based designs have two windows). Table 2 shows the comparison, including some basic assumptions about various major

corrections. The values of N_0 are quoted for a full ring (dip angle 0°), and the prediction of the number of photoelectrons is quoted for a dip angle of 25°; Table 2 also includes the experimental results [39, 42, 46]. Clearly, the TEA-based photocathode is very interesting indeed, especially considering the latest Cornell test results [46]. TMAE is at a disadvantage because of the necessity of having two windows (for C_6F_{14} radiator), and its poor photon absorption length - see Table 2. However, the chromatic behavior of the C_6F_{14} liquid makes TMAE still the best in terms of the π/K separation capability (~4 σ π/K separation is predicted at ~3.1 GeV/c at θ_{dip}=25°).

CONCLUSIONS

The detection of single electrons using gaseous devices is rather tricky. To many involved in the planning of large experiments, it was not clear initially whether it would be possible to detect single photo-electrons on such a large scale with good efficiency. It has required a great deal of effort, and many mistakes have been made along the way. Drift chambers and TPC's, which are commonly used today for tracking, have required many iterations to become successful and accepted. If a similar number of iterations was allowed the gaseous photon detectors, they would improve and prove themselves to be reliable particle identification devices. Considering that photon detectors have finished only their first iteration, they have performed remarkably well, especially in fixed target applications. I would add the following comments :

a. High wire gains in single gap MWPC photon detectors, such as described in chapter 3.1, should probably be avoided in future. High gas gain operation adversely affects the wire aging rate, the probability of sparking, cross-talk, the chance of Malter currents, and makes it necessary to surround the wire with complicated electrode "blind" structure to limit the avalanche photon feedback rate. It is also important to limit the thickness of the detector presented to traversing particles in order to reduce dE/dx deposits. A good solution is a thin detector combining very low gas gain with slow, low noise, electronics connected to each pad, as used in the Cornell prototype [46]. The RD-26 CERN prototype [42] has pioneered this philosophy, which trades high gain and speed for small gain, low noise and geometrical pixelization. In principle, all three photocathodes, i.e. TMAE, TEA and CsI, can be used with this method. It may be future direction for non-LHC applications.

b. Detector operation at very low total gas gain (~$5x10^4$), results in pulse height spectra having θ=0. The only way to have good single electron efficiency (>95%) is to have electronics with very low noise (in the range of ~500 e^- rms). This may not be trivial to achieve in the final systems. More work in this area is needed, but it is a direction worth pursuing.

c. Gaseous detectors may not be adequate for LHC applications. This is an area where they might end up being replaced by solid state devices, such as hybrid PM's. One device which may possibly try to compete in some specialized applications is a single gap, low pressure, low gain, parallel plate gap detector operating with a TEA-based gaseous photocathode. However, this would require the development of a new fast, low noise amplifier.

d. At high gas gain, single gap MWPC detectors, although more resistant to sparking due to their amplification nonlinearity, are more sensitive to secondary photo-electrons compared to single or multiple parallel gap amplification detectors. A combination of the two, especially at low pressure, is a good solution, as pioneered by the CERES [38] and HELIOS [52] prototypes.

e. The author favors gaseous photocathodes (TMAE or TEA) over solid ones in MWPC detectors, because they are continuously refreshed, have high quantum efficiency and because the techniques used to clean the gases have been perfected over many years.

f. The TEA photocathode is possibly "re-emerging" as an interesting candidate, because of a relatively high quantum efficiency, small photon absorption length and the possibility of operation at room temperature. TEA is a more tightly bound molecule than is TMAE, and so better wire aging behavior would be expected. However, the high photon energy needed to photo-ionize TEA requires special attention from the point of view of possible window contamination problems.

g. Solid photocathodes, such as CsI, were meant to be used for the very high rate applications at LHC because of their expected fast response. This is now doubtful after the experience of the College de France LHC-B prototype [40], and since several aging tests have revealed a too-rapid degradation of the CsI photocathode quantum efficiency for such applications. Such photocathodes do exist in phototubes; however, there, large photo-currents across the photocathode volume do not occur. This is not the case in gaseous detectors. A great deal more R&D effort will be needed in order to learn how to operate such photocathodes successfully in a gaseous detector placed in a 4π-solid angle experiment, which allows limited access and lasts ~5 years.

h. When the anode-cathode gap is small (0.4-0.8 mm), the anode wire diameter should be kept around ~15 μm in order to have uniform gain around the wire and to have stable operation. However, anode wire diameters below 10 μm should be avoided in order to prevent wire-breaking problems. Larger anode wire diameter (30-50 μm) reduces the wire aging rate, however it should be used in symmetrical geometries only (such as tubes) in order to avoid gain variation around the wire.

i. TMAE anode wire aging is not so threatening if anode wire of larger diameter is used (30-50 μm). A gain drop of 30-50% after few mC/cm could be compensated for by adjusting the high voltage. In high rate applications, the use of carbon wires is recommended in conjunction with a system for heating the wires by sending a small current through them [18].

j. It may be necessary to add a small amount of water (~20ppm) to prevent charging effects in TMAE systems which are not opened to air for years, and which have been carefully designed to remove water in the first place [18]. The problem may be relevant for all photo-detectors, since photo-cathode materials are generally good insulators. It is necessary to add water to many drift chambers to prevent similar charging effects.

k. Recent progress in the calculational capability of analytical chemistry should be utilized to pursue new photocathode concepts. It is hard to believe that all conceivable photocathode candidates have

been tried to this point.

l. Recently, many non-gaseous devices have appeared on the market. It remains to be seen how successful they will be in replacing gaseous detectors. If they do work, they will remove the great fun some of us have had creating them on our knees at home.

ACKNOWLEDGEMENTS

It proved surprisingly difficult to collect the detector information from various experiments in an orderly tabular form. I appreciate the help which I have received from many people. I would like to thank especially F. Piuz for several good suggestions, many interesting discussions about single electron pulse height spectra, and lots of laughs about driving on the wrong side (i.e. the right side) of the road during his vacation in Scotland ...

FIGURE CAPTIONS

1. The quantum efficiency of TMAE and CsI. The graph also shows the transmission of 1 cm of C_6F_{14} liquid, which is a typical radiator in the CRID detectors, and defines the short wavelength acceptance edge [5].
2. The analysis of pulse shapes in the CRID barrel detector using single photo-electrons from UV fiber data : (a) pulse height spectrum measured with the low threshold (~$8x10^3$ e^-), and with the real threshold of ~$2\text{-}3x10^4$ e^- used in the 1994 run (dashed line), (b) details of the fit near the pedestal with the two thresholds shown [data (closed circles), overall fit (crosses), Gaussian contribution (open circles), Polya contribution (dots)], and (c) the effect of threshold on the single electron efficiency, as evaluated using equation (2).
3. Examples of (a) well quenched single electron pulses in CF_4 gas, and (b) poorly quenched pulses using CF_4+TMAE gas (bubbler at 40°C; the detector at 50°C), which demonstrate avalanche breeding [5].
4. Quenching seen through the single electron spectra [5] in (a) 80% CF_4+20% iC_4H_{10} (no TMAE; detector at 25°C), $\theta > 0$; (b) 80% CF_4+20% iC_4H_{10} +TMAE (bubbler at 40°C; detector at 50°C), $\theta < 0$; (c) 68% CF_4 +32% iC_4H_{10} +TMAE (bubbler at 40°C; detector at 50°C), $\theta \sim 0$; (d) 63.5% CF_4 +36.5% iC_4H_{10}+TMAE (bubbler at 40°C; detector at 50°C), $\theta > 0$. The solid line indicates an exponential shape.
5. The charge collection in two extreme examples of geometries [14]: (a) typical MWPC geometry, (b) only ~20% of the charge is collected in the first 20 ns in the MWPC, (c) micro-gap geometry (MGC), (d) close to ~95% of the charge is collected in the same period in the MGC.
6. TMAE wire aging results [5] in 80%CF_4+20%iC_4H_{10} gas (no TMAE; detector at 24°C; open triangles) with a 50 μm diameter gold plated tungsten wire; the same, but with TMAE (15°C bubbler; open circles); in 80%CF_4+ 20%iC_4H_{10} gas with TMAE (40°C bubbler; detector at 47.6°C; open squares) with 33 μm diameter carbon wire; in C_2H_6 with TMAE (27°C bubbler; detector at 40°C; open diamonds) with 7 μm diameter carbon wire (CRID Barrel condition).
7. TMAE wire aging test results [18] with 33 μm wire diameter (bubbler at 40°C, detector at 50°C) for : (a) C_2H_6 (open downward triangle, closed downward triangle, closed circles), CH_4 (closed diamond, closed squares), 15% CO_2+85% C_2H_6 (closed upward triangles, open upward triangles) and compared to "old" results for CH_4 gas (open squares, bubbler at 40°C; detector at 50°C); (b) 80% He+20% iC_4H_{10} (closed circles, closed downward triangles), 60% He+40% iC_4H_{10} (open squares), iC_4H_{10} (closed squares), 50%He+ 50% C_2H_6 (open diamonds).
8. TMAE wire aging results in the Omega experiment [20] : (a) the pulse height spectrum on new wire prior to the 1991 run, (b) the same after the 1991 run accumulating a charge dose ~1 mC/cm while not gating.
9. The electrode blinds used in TMAE-based detectors for : (a) the DELPHI prototype [29], (b) the DELPHI barrel [31], (c) CRID barrel [33] and (d) OMEGA [35] experiments.
10. Two different solutions for the electrode blinds in endcap detectors operating with the E x B effect : (a) DELPHI [32] and (b) SLD CRID [34].
11. The TMAE-based Fast Drift CRID detector using short drift cells and small height to minimize track dE/dx deposits and thus to limit photon feedback [37].
12. The triple amplification scheme using two parallel gaps and one MWPC stage in the CERES experiment [38]. The non-linear amplification of the wires in the MWPC last stage successfully kept the sparking rate within an acceptable limit .
13. The College de France prototype geometry with pad readout for the TEA-based gaseous photocathode[39]; in the case of the "CsI" prototype, the CsI solid photocathode was evaporated onto the pad structure [40].
14. Single electron pulse height spectra in : (a) the RD26 CERN prototype [42] operating with CH_4 gas at 1 atm, 1950 kV, and using Cherenkov ring photoelectrons ($\theta \sim 0$); (b) the same, but at increased voltage 2100 V($\theta < 0$); (c) the Princeton prototype operating with C_2H_6 at 735 Torr, and using a UV-lamp as the source of photoelectrons ($\theta > 0$).
15. The "room temperature" TMAE-based prototypes with individual cell type blinds : (a) the JETSET [49] detector, and (b) the new College de France "TMAE" [51] prototype using the wire structure of Fig. 13.
16. Single electron pulse height spectra using Cherenkov ring hits in (a) the CERES detector [38] operating in 94% He+ 6% C_2H_6 gas at normal pressure ($\theta < 0$; the solid line indicates an exponential shape), (b) the HELIOS "pad" detector [52] operating at low pressure of 40 Torr in 80% C_2H_6 +20% Ar gas ($\theta > 0$), and (c) single electron spectrum from the Be X-ray

conversions in the low pressure two-stage parallel plate gap detector [56], operating with an average total gain ~$7x10^6$ in 80% C_2H_6+20% Ar gas at 10.3 Torr (θ=+0.4; the solid curve is the Polya fit).

17. The HELIOS prototype [56] with an optical CCD-based readout using three parallel amplification gaps and a gate. Two parallel gaps were used to develop the charge and one was used to maximize the photonic excitations.
18. (a) The Munich micro-strip chamber [59], and (b) the INFN Pisa micro-gap chamber [60].
19. Single electron pulse height spectra in the micro-gap chamber [60] operating at 1 atm using UV lamp photons : (a) gain obtained mostly from the drift region (V_{drift}=-3550 V, V_{a-c}=-50 V; θ>0), (b) gain obtained mainly from the strip region (V_{drift}=-3000 V, V_{a-c}=-400 V; θ~0).
20. Single electron pulse height spectra in the micro-strip chamber [61] operating at the low pressure of 30 Torr in C_2H_6 using UV lamp photons and using both strip and gap amplification.
21. The schematic description of the DIRC detector with the water tank solution using standard photomultipliers [62].
22. The schematic description of the DIRC detector without the water tank solution [70] using multi-anode PM's [65].
23. (a) The concept of the hybrid PM with only PIN diodes inside the gas envelope; the electronics is outside[66]; (b) a typical pulse height spectrum illustrating the hybrid PM's superb capability in measuring multiple electrons.
24. The concept of the hybrid PM where both the detector pixel chip, and the electronics chip (which is bonded to the pixel chip) are inside the gas envelope [67].
25. The concept of the electron multiplier using glass micro-balls (MSP) [69].

DISCLAIMER

REFERENCES

[1] J. Seguinot and T. Ypsilantis, Nucl.Instr.&Meth., A343(1994)1.
[2] J. Seguinot and T. Ypsilantis, Nucl.Instr.&Meth., A343(1994)30.
[3] A. Breskin, "CsI : History & Mystery", invited contribution to this workshop.
[4] A.H. Cookson and T.J. Lewis, Brit.J.Appl.Phys. 17(1966)1473; J. Byrne, Proc.Roy.Soc.Edin. 66A(1962)33; L. Lansiart and J.P. Morucci, J.Phys.Radium Suppl. 6, no.23(1962)A102.
[5] J. Va'vra, J. Kadyk, J. Wise and P. Coyle, SLAC-PUB-95-6783, and Nucl.Instr. &Meth., A324(1993)113.
[6] J. Friese, R. Gernheauser, G. Montermann and K. Zeitelhack, Physik-Department E12, TU-Munchen, Germany, unpublished report.
[7] H. Raether, "Electron avalanches and breakdown in gases", p.60, Butterworths, London, 1964.
[8] H. Schlumbohm, Z. Phys., 151(1958)563 and 152(1958)49.
[9] W. Legler, Z. Naturforsch 16a(1961)253.
[10] G.D. Alkhazov, Nucl.Instr.&Meth., 89(1970)155.
[11] H. Genz, Nucl.Instr.&Meth., 112(1973)83.
[12] R. Arnold et. al., Nucl.Instr.&Meth., A343(1992)465.
[13] Gatti-Manfredi-Radeka, Riv. Nuovo Cimento 9(1986) and Ann. Rev. Nucl. Part. Sci. (1988)217.
[14] R. Bellazzinni and M.A. Spezziga, Riv. Nuovo Cimento 12(1994).
[15] AMPLEX chip : E. Beuville, K. Borer, E. Chesi, E.H.M. Heijne, P. Jarron, B. Lisowski and S. Singh, Nucl.Instr.&Meth., A288(1990)157.
[16] VIKING chip : E. Nygard, P. Aspell, P. Jarron, P. Weilhammer and K. Yoshioka, Nucl.Instr.&Meth., A301(1991)506.
[17] J. Va'vra, IEEE Trans. Nucl. Sci., NS 34, No.1, p.486, February 1987; CRID Note #36, SLAC, 1987 and IEEE Trans. Nucl. Sci., NS 35, No.1, p.487, February 1988.
[18] J. Va'vra, SLAC-PUB-95-6759 and the Vienna Wire Chamber Conference, 1995.
[19] C. Woody, IEEE Trans. Nucl. Sci., NS 35, No.1, p. 493, February 1988.
[20] K. Martens et.al., Nucl.Instr.&Meth., A343(1994)258.
[21] L. Malter, Phys.Rev. 50(1936), and Guentherschultze, Z.Phys. 86(1933)778.

[22] J. Va'vra, A. Breskin, A. Buzultskov, R. Chechik, E. Shefer, " Resistivity of the CsI photocathode and its impact on high rate dependence of the gaseous MWPC detectors", to be published.
[23] H. Raether, Z. Phys. 112(1939)464.
[24] P. Fonte, V. Peskov and F. Sauli, Nucl.Instr.&Meth., A305(1991)91.
[25] N.W. Ashcroft, N.D. Mermin, Solid State Physics, p. 621, N.Y., Holt, Rinehart and Winston, 1976.
[26] J. Va'vra, A. Breskin, A. Buzultskov, R. Chechik, E. Shefer, " Aging of the CsI-based photocathode in the gaseous MWPC detectors", to be published.
[27] P. Krizan et. al., IJS report, IJS-DP-7087, October 1994.
[28] C. Lu et. al., Princeton preprint HEP/95-1.
[29] R. Arnold et. al., Nucl.Instr.&Meth., A270(1988)255.
[30] O. Botner et.al., Nucl.Instr.&Meth., A257(1987)580, L.O. Eek et.al., IEEE Trans. Nucl. Sci., NS 31, (1984)949, and K. Fransson, Ph.D. thesis, ISBN 91-7900-908-4, Uppsala 1990.
[31] D. Bloch et. al., Nucl.Instr.&Meth., A273(1988)847, and W. Adam et.al., Nucl.Instr.& Meth., A343(1994)68, and M. Darkos and D. Loukas, Nucl.Instr.&Meth., A302(1991)241 .
[32] W. Adam et.al., Nucl.Instr.&Meth., A338(1994)284.
[33] D. Aston et.al., Nucl.Instr.&Meth., A283(1989)582, K. Abe et.al., Nucl.Instr.&Meth., A343(1994)74 and K. Abe et.al., 5-th International Conference on Instrumentation for Colliding Beam Physics, Novosibirsk, Russia, March 15, 1990.
[34] K. Abe et.al., SLAC-PUB-95-6693.
[35] H.-W. Siebert, Nucl.Instr.&Meth., A343(1994)60, U. Mueller et.al., CERN-PPE/95-117, and U. Mueller private communication.
[36] S. Swordy, private communication, J. Buckley et.al., The Astrophysical Journal, 429 (1994) 736, and S. Swordy, Nucl.Instr.& Meth., A343(1994)52.
[37] J. Va'vra, B-Factory note #68, 1994.
[38] R. Baur et.al., Nucl.Instr.&Meth., A343(1994)87 and Nucl.Instr.&Meth., A343(1994)231.
[39] J. Seguinot et.al., Nucl.Instr.&Meth., A350(1994)430, R. Arnold et.al., Nucl.Instr.&Meth., A314(1992)465, and M. French et.al., Nucl.Instr.&Meth., A324(1993)511.
[40] J. L. Guyonnet, presentation at RICH Workshop, Uppsala, Sweden, June 11-18, 1995.
[41] J. Krizan et.al., private communication, and J. Krizan et.al., IJS Report, IJS-DP-7087, 1994.
[42] F. Piuz et.al., private communication, and "Photocathodes", invited talk at RICH Workshop, Uppsala, Sweden, June 11-18, 1995; A. Bream et.al., Nucl.Instr.&Meth., A343(1994)163.
[43] P. Besson, private communication.
[44] J. Friese, private communication.
[45] C. Lu, private communication, and presentation at RICH Workshop, Uppsala, Sweden, June 11-18, 1995.

[46] S. Playfer, private communication, and presentation at RICH Workshop, Uppsala, Sweden, June 11-18, 1995.
[47] P. Carlson et.al., Nucl.Instr.&Meth., A343(1994)198.
[48] S. Swordy, private communication.
[49] R.T. Jones, M. Price and H. Wirth, Nucl.Instr.&Meth., A343(1994)208.
[50] J. Krizan, private communication.
[51] T. Ypsilantis, presentation at RICH Workshop, Uppsala, Sweden, June 11-18, 1995.
[52] A. Fisher et.al., IEEE Trans.Nucl.Sci., Vol.35, p.432, No.1, Feb. 1988.
[53] B. Surrow et.al., Nucl.Instr.&Meth., A355(1995)342.
[54] A. Akkerman et.al., Nucl. Instr.&Meth., A315(1992)82.
[55] S. Kwan and D. Anderson, Nucl. Instr.&Meth., A309(1991)190.
[56] A. Pansky, private communication.
[57] A. Breskin et.al., Nucl.Instr.&Meth., A273(1988)798, and IEEE Trans.Nucl.Sci., Vol.35, p.404, No.1, Feb. 1988.
[58] J. Baechler et.al., Nucl.Instr.&Meth., A324(1993)449, Nucl.Instr.&Meth., A343(1994)288, and private communication with G. Paic.
[59] K. Zeitelhack et.al., Nucl.Instr.&Meth., A351(1994)585; C. Erbe and J. Friese, private communication.
[60] R. Bellazzini, private communication, and contribution to the Vienna Wire Chamber Conference, 1995.
[61] E. Shefer, private communication.
[62] B. Ratcliff, SLAC-PUB-5853, 1992, P. Coyle et.al., Nucl.Instr.&Meth., A343(1994)292, and B. Ratcliff, "RICH in future experiments", invited talk at RICH Workshop, Uppsala, Sweden, June 11-18, 1995.
[63] M. Pommot Maia et.al., FERMILAB-Pub-92/155.
[64] K. Kuroda, D. Sillou and F. Takeutchi, Rev. Sci. Instrum., 52(1981)337.
[65] H. Matsuura, Y. Hasegawa, M. Ito and H. Kyushima, Hamamatsu Photonics K.K. Electron Tube Center, contribution to SPIE's 1995 Int. Symp. on Opt.Sci., Eng. and Instr., 1995.
[66] R. DeSalvo, CLNS 87-92, Cornell University, Ithaca, NY; see also R. DeSalvo et. al., Nucl.Instr.&Meth., A315(1992)375.
[67] C. D'Ambrosio et.al., the Vienna Wire Chamber Conference, 1995, and E. Heijne et.al., The RD-19 Collab.
[68] J. Seguinot, P. Weilhammer and T. Ypsilantis, LHC R&D project to develop HPD with 256 pixels
[69] El-Mul Technologies Ltd., Rehovot, Israel.

[70] B. Ratcliff, private communication.
[71] CERN Letter of intent, CERN/LHCC 95-5.

TABLE 1. Design parameters of the gaseous photon detectors a)

DETECTOR	Photo-cathode	Carrier gas	Gas pressure	Bubbler temp.	Detector temp.	Anode wire diameter	Anode cathode distance	Anode cathode gap	Anode wire spacing	Anode cathode coupling
DELPHI prototype [29]	TMAE	75% CH_4+ 25% C_2H_6	1 atm	27 °C	40 °C	20 μm	1.0 mm	sym.	2.54 mm	0.78
UA2-RICH [30]	TMAE	CH_4	1 atm	27 °C	33 °C	20 μm	1.13 mm	sym.	2.54 mm	
DELPHI barrel [31]	TMAE	75% CH_4 + 25% C_2H_6	1 atm	27 °C	40 °C	20 μm	0.5 mm	assym.	2.62 mm	0.60
DELPHI endcap [32]	TMAE	C_2H_6	1 atm	25 °C	30 °C	20 μm	0.7 mm	assym.	2.62 mm	0.70
SLD CRID barrel [33]	TMAE	C_2H_6	1 atm	27 °C	34 °C	7 μm	1.4 mm	assym.	3.18 mm	-
SLD CRID endcap [34]	TMAE	C_2H_6	1 atm	23 °C	30 °C	7 μm	1.4 mm	assym.	3.18 mm	-
OMEGA RICH [35]	TMAE	85% CO_2 + 15% C_2H_6	1 atm	30 °C	40 °C	15 μm	1.15 mm	sym.	2.54 mm	-
RICH-I [36]	TMAE	C_2H_6	1 atm	12 °C	20 °C	25 μm	1.5 mm	assym.	4.0 mm	-
Fast DRIFT CRID [37]	TMAE	C_2H_6	1 atm	40 °C	45 °C	33 μm	0.8 mm	assym.	5.0 mm	-
CERES [38]	TMAE	94% He+ 6% C_2H_6	1 atm	40 °C	50 °C	30 μm	2 & 4 mm	sym.	2 & 3 mm	
College de France [39]	TEA	CH_4	1 atm	17 °C	30 °C	15 μm	0.5 mm	assym.	1.27 mm	0.80
College de France [40]	CsI	CH_4	1 atm	-	ambient	15 μm	0.5 mm	assym.	1.27 mm	0.80
HERA-B (CsI) [41]	CsI	CH_4	1 atm	-	ambient	15 μm	0.66 mm	assym.	2.5 mm	0.70
RD-26 - CERN [42]	CsI	CH_4 (99.95% purity)	1 atm	-	ambient	20 μm	2.0 mm	sym.	4.0 mm	
RD-26 - Saclay [43]	CsI	CH_4	1 atm	-	ambient	20 μm	2.0 mm	sym.	4.0 mm	0.45
RD-26 - Munich [44]	CsI	CH_4	1 atm	-	ambient	20 μm	1.2 mm	asym.	3.0 mm	0.76
Princeton [45]	CsI	C_2H_6	1 atm	-	ambient	20 μm	5.0 mm	sym.	2.54 mm	0.29
Cornell prototype [46]	TEA	CH_4	1 atm	15 °C	ambient	20 μm	1.0 mm	sym.	2.5 mm	0.75
CAPRICE [47]	TMAE	C_2H_6	1 atm	40 °C	48 °C	15 μm	2.0 mm	sym.	4.0 mm	
RICH-II [48]	TMAE	C_2H_6	1 atm	12 °C	25 °C	25 μm	2.0 mm	assym.	4.0 mm	
JETSET [49]	TMAE	25% He+ 75% C_2H_6	1 atm	20 °C	ambient	50 μm	4.0 mm	sym.	8.0 mm	-
HERA-B (TMAE) [50]	TMAE	CH_4	1 atm	21 °C	ambient	25 μm	4.0 mm	sym.	8.0 mm	-
College de France [51]	TMAE	CH_4/iC_4H_{10} mix	1 atm	-	ambient	15 μm	0.5 mm	assym.	1.27 mm	0.80
HELIOS - pads [52]	TMAE	20% Ar + 80% C_2H_6	40 Torr	35 °C	45 °C	20 μm	2.0 mm	sym.		
PHENIX [53]	CsI	C_2H_6	35 Torr	-	ambient	18 μm	1.6 mm	sym.		
HELIOS - optical [56]	TMAE	20% Ar + 80% C_2H_6	40 Torr	34 °C	45 °C	-	4.0 mm	sym.	-	-
NA35 - optical [57]	TMAE	93% He+ 7% C_2H_6	1 atm	48 °C	55 °C	-	4.0 mm	sym.	-	-
Munich microstrip [58]	CsI (refl.)	85% Ar + 15% C_2H_6	1 atm	-	ambient	10 μm strip	150 μm	assym.		0.20
Pisa microgap [59]	CsI (trans.)	85% Ne + 15% DME	1 atm	-	ambient	5 μm strip	5 μm	assym.		1.0
Weizmann microstrip [60]	CsI (trans.)	iC_4H_{10}	10 Torr	-	ambient	10 μm strip	55 μm	assym.		

b)

DETECTOR	Anode wire material	Cathode material	Coordinate along the wire	Front electronics	Preamplifier gain	Electronics overall noise (rms)
DELPHI prototype [29]	Au plated W	s.s. tube	5 mm tube segments	LeCroy TRA403	95 mV / μA (100 Ω)	~ 7500 e^-
UA2-RICH [30]	Au plated W	s.s. tube	5 mm tube segments	NE 592 D	70 mV / μA (100 Ω)	~ 3200 e^-
DELPHI barrel [31]	Au plated W	Au plated Cu	4 mm wide strips	CERN	100 mV / μA (100 Ω)	~ 4000 e^-
DELPHI endcap [32]	Au plated W/Rh	Au plated Cu	5 mm wide strips	CERN - LOG	300 mV / μA (100 Ω)	~ 1800 e^-
SLD CRID barrel [33]	Carbon	Ni plated Al	charge division	SLAC	17 mV / fC	~ 2300 e^-
SLD CRID endcap [34]	Carbon	Ni plated Al	charge division	SLAC	17 mV / fC	~ 2300 e^-
OMEGA RICH [35]	Au plated W	Ni plated W	No measurement done	VV44 Heidelberg	25 mV / μA (70 Ω)	~ 350 e^-
RICH-I [36]	Au plated W	Brass	No measurement done	Nanometric N277C	22 mV / μA (100 Ω)	~ 10000 e^-
Fast DRIFT CRID [37]	Carbon	Cr plated quartz	charge division	SLAC	17 mV / fC	~ 2500 e^-
CERES [38]	Au plated W	Paint on Cu	pad pitch 2.74&7.62	CAMEX	8 mV / fC	~ 1750&2200 e^-
College de France [39]	Au plated W	Au plated Cu	5.3 x 6.6 mm^2 pads	RAL110&RAL111	1370 mV / μA (100 Ω)	~ 1250 e^-
College de France [40]	Au plated W	Au plated Cu	5.3 x 6.6 mm^2 pads	RAL110&RAL111	1370 mV / μA (100 Ω)	~ 1250 e^-
HERA-B (CsI) [41]	Au plated W	Sn/Pb plated Cu	7.5 x 7.5 mm^2 pads	Lubljana	8.3 mV / fC	~ 1000 e^-
RD-26 - CERN [42]	Au plated W	Au plated Cu	8 x 8 mm^2 pads	AMPLEX	15 mV / fC	~ 1500-2000 e^-
RD-26 - Saclay [43]	Au plated W	Ni plated Cu	8 x 8 mm^2 pads	AMPLEX	15 mV / fC	~ 1500-2000 e^-
RD-26 - Munich [44]	Au plated W	Au plated Cu	6 x 6 mm^2 pads	AMPLEX	15 mV / fC	~ 2000 e^-
Princeton [45]	Au plated W	Al/Au plated Cu	8.1 x 8.1 mm^2 pads	AMPLEX	15 mV / fC	~ 1600 e^-
Cornell prototype [46]	Au plated W	Au plated Cu	7.6 x 7.6 mm^2 pads	VA2 VIKING chip	70 mV / fC	~ 400 e^-
CAPRICE [47]	Au plated W	Au plated Cu	8 x 8 mm^2 pads	AMPLEX	15 mV / fC	~ 1250 e^-
RICH-II [48]	Au plated W	Au plated Cu	10 x 10 mm^2 pads	AMPLEX	15 mV / fC	
JETSET [49]	Au plated W	Refl. Al	8 x 8 mm^2 cells	Fujitsu MB43468	25 mV / fC	~ 2000 e^-
HERA-B (TMAE) [50]	Au plated W	Refl. bronze	8 x 8 mm^2 cells	ARGUS μVDC		
College de France [51]	Au plated W	Au plated Cu	5.3 x 6.6 mm^2 pads	RAL110&RAL111	1370 mV / μA (100 Ω)	~ 1250 e^-
HELIOS - pads [52]	Au plated W	Au plated Cu	2 mm dia. pads	MICROPLEX	10 mV / fC	~ 4000 e^-
PHENIX [53]	Au plated W	Al/Ti plated Cu	2.54 x 2.54 mm^2 pads		0.5 mV / fC	
HELIOS - optical [56]	s.s. mesh	s.s. mesh	-	-	-	-
NA35 - optical [57]	s.s. mesh	s.s. mesh	-	-	-	-
Munich microstrip [58]	Al	Al	6.3 x 6.3 mm^2 pads	AMPLEX	15 mV / fC	~ 2400 e^-
Pisa microgap [59]	Cr	Cr	25 x 3.2 mm^2 pads	Laben 5231&5185	6 mV / fC	~ 4400 e^-
Weizmann microstrip [60]	Cr	Cr	No pads yet	ORTEC VT110	10 mV / μA (50 Ω)	

c)

DETECTOR	Detector charge integration time	Wire gain	Gain	Gate width during the gain test only	Photon feedback control	Feedback rate (second hit per aval.)	Quenching based on the PH spectrum
DELPHI prototype [29]	~ 10-20 ns	~ 4.7 x 10^5 (1625 V)	total	10-20 ns	tube walls	~0.8 %	θ > 0 (?)
UA2-RICH [30]	~ 10-20 ns	~ 3 x 10^5	visible	10-20 ns	tube walls		
DELPHI barrel [31]	~ 10-20 ns	~ 1.9 x 10^5 (1450 V)	visible	~ 400 ns	Al_2O_3 blinds	~4.5 %	θ > 0
DELPHI endcap [32]	~ 10-20 ns	~ 10^5 (1650 V)	visible	10-20 ns	G-10 blinds		
SLD CRID barrel [33]	~ 65 ns	~ 2.5 x 10^5 (1500 V)	total	~ 420 ns	Cu-Be blinds	< 1 %	θ > 0
SLD CRID endcap [34]	~ 65 ns	~ 3 x 10^5 (1500 V)	total	~ 420 ns	Cu-Be blinds		θ > 0
OMEGA RICH [35]	~ 10-20 ns	1- 2 x 10^5 (1750 V)	visible	10-20 ns	Al_2O_3 blinds	~2 %	θ > 0
RICH-I [36]	~ 25 ns	~ 8 x 10^4 (2200 V)	visible	~ 25 ns	Brass blinds	~2-3 %	θ ~ 0
Fast DRIFT CRID [37]	~ 65 ns	~ 6-8 x 10^4 (1625 V)	total	~ 640 ns	small dE/dx	-	θ ~ 0
CERES [38]	~ 50-100 ns	~ 2 - 4 x 10^5	total	-	3-stage ampl.	< 1 %	θ < 0
College de France [39]	~ 10-20 ns	~ 4 x 10^5	total	10-20 ns	gas & gain		θ ~ 0
College de France [40]	~ 10-20 ns	< 10^5	total	10-20 ns	gas & gain		θ ~ 0
HERA-B (CsI) [41]	~ 40 ns	~ 10^5	total	-	gas & gain	~10 %	θ < 0
RD-26 - CERN [42]	~ 500-600 ns	6- 8 x 10^4 (2000 V)	total	-	gas & gain		θ ~ 0
RD-26 - Saclay [43]	~ 500-600 ns	~ 10^5	total	-	gas & gain		θ ~ 0
RD-26 - Munich [44]	~ 500-600 ns	~ 1.6 x 10^5 (2600 V)	visible	500-600 ns	gas & gain		θ < 0
Princeton [45]	~ 500-600 ns	~ 4.6 x 10^5 (4100 V)	total	-	gas & gain		θ > 0
Cornell prototype [46]	~ 1000 ns	2 - 3 x 10^4 (1450 V)	visible	~1000 ns	gas & gain		θ ~ 0
CAPRICE [47]	~ 500-600 ns	~ 10^5 (1825 V)	visible	500-600 ns	gas & gain	<10 %	θ > 0
RICH-II [48]	~ 500-600 ns	~ 10^5	visible	500-600 ns	gas & gain	~2-3 %	θ ~ 0
JETSET [49]	~ 10-20 ns	2 - 4 x 10^5	total	-	cell walls		θ > 0
HERA-B (TMAE) [50]		~ 10^6	total	-	cell walls		
College de France [51]	~ 500-600 ns				G-10 blinds		
HELIOS - pads [52]	< 1000 ns	< 10^6	total	-	2-stage ampl.		θ > 0
PHENIX [53]					gas & gain		θ ~ 0
HELIOS - optical [56]	-	~ 10^7	total	-	3-stage ampl.		-
NA35 - optical [57]	-	~ 10^7	total	-	2-stage ampl.		-
Munich microstrip [58]	~ 500-600 ns	~ 3 x 10^4	visible	1 - 2 μs	gas & gain		θ < 0
Pisa microgap [59]	~ 10-20 ns	~ 3.6 x 10^5	total	-	gas & gain		θ ~ 0
Weizmann microstrip [60]	< 10 ns	?			gas & gain		θ < 0

Table 2 - Expected N_0 Performance for gaseous detectors considered for the B-factory.
(Note that the light does not escape from the LiF radiator at $\theta_{dip}=0^o$)

Parameter	CAPRICE style pad detector (TMAE)	Fast Drift CRID (TMAE)	Fast RICH with TEA	Fast RICH with CsI
Assumed design	two windows	two windows	one window	one window
Photocathode	TMAE-40°C	TMAE-40°C	TEA	CsI
Source of Q.E. of TMAE / TEA / CsI	Holroyd	Holroyd	Sequinot	Breskin
Source of transmission curve for LiF or C_6F_{14} (1 cm path)	SLD CRID	SLD CRID	Sequinot	SLD CRID
Source of transmission curve for quartz or CaF_2 windows (~4 mm path)	SLD CRID	SLD CRID	Sequinot	SLD CRID
Assume photon transmission due to losses in gaps between the chamber cells	0.95	0.85	1.0	0.95
Assume photon transmission losses due to electrode strips on the quartz and field wires	0.95	0.87	0.93	0.98
Assume fraction of photons converting to photoelectrons due to a finite size of TPC (TMAE or TEA absorption length ℓ_{abs})	0.65 (ℓ_{abs}~6 mm)	0.96 (ℓ_{abs}~6 mm)	1.0 (ℓ_{abs}~0.6 mm)	1.0 (ℓ_{abs}~0 mm)
Assume chamber efficiency	0.90	0.9	0.97	0.9
Assume average correction due to loss of electrons during the drift	1.0	0.99	1.0	1.0
Total fraction of photoelectrons contributing to the "final efficiency", compared to the "starting efficiency", which is given by transmissions of quartz / CaF_2 /C_6F_{14} & Q.E. of TMAE /TEA/ CsI	**0.53**	**0.63**	**0.90**	**0.84**
Mean photon energy	6.50 eV	6.50 eV	8.36 eV	6.70 eV
Mean refraction index	1.27802 [2]	1.27802 [2]	1.505 [2]	1.2799 [2]
Mean Cherenkov angle (β = 1 particle)	38.51°	38.51°	48.19°	38.62°
Radiator	C_6F_{14}	C_6F_{14}	LiF	C_6F_{14}
Radiator length	1 cm	1 cm	1 cm	1 cm
Expected N_0 - "starting efficiency" (for "full" ring at $\theta_{dip}=0^o$)	**~ 81 cm^{-1}**	**~ 81 cm^{-1}**	**~ 65 cm^{-1}**	**~ 45 cm^{-1}**
Expected N_0 - "final efficiency" (for "full" ring at $\theta_{dip}=0^o$)	**~ 43 cm^{-1}**	**~ 51 cm^{-1}**	**~ 59 cm^{-1}**	**~ 38 cm^{-1}**
Expected "final" number of photo-electrons per "partial" ring at $\theta_{dip}=25^o$ (β = 1 particle & simple events)	**10**	**12**	**12-13**	**9**
Measured number of photo-electrons per "partial" ring at $\theta_{dip}=25^o$ (β = 1 particle & simple events)	**-**	**-**	**11.2 [39] ~12-13 [46]**	**8-10 [42]**

d)

DETECTOR	Anode wire single electron detection efficiency	Cathode pad single electron detection efficiency	Detector publishing physics ?	Comment
DELPHI prototype [29]	> 97 %	> 92 %	Prototype	A very large total wire gain used (>10^6); TMAE supports it.
UA2-RICH [30]	> 90 %	> 30 %	Yes	
DELPHI barrel [31]	> 96.7 %	> 86 %	Yes	A moderately high total wire gain used (>6 x 10^5)
DELPHI endcap [32]	> 98 %	> 96 %	Yes	Logarithmic pre-amplifier response implemented
SLD CRID barrel [33]	> 82 %	-	Yes	7 μ m carbon wire proved to be too fragille
SLD CRID endcap [34]		-	Yes	
OMEGA RICH [35]	> 95 %	-	Yes	Gating is necessary to limit the wire charge dose to reduce aging
RICH-I [36]	> 40 %	-	Yes	Used in a balloon flight; the entire load used 340 Watts.
Fast DRIFT CRID [37]	> 50 %	-	Prototype	Not sufficient gain obtained in this particular configuration
CERES [38]	-	> 90 %	Yes	MWPC stage added to reduce the sparking problems
College de France [39]		> 97 %	Prototype	A very large total wire gain used (>10^6); TEA supports it.
College de France [40]			Prototype	CsI doesn't support the required high wire gain; small efficiency.
HERA-B (CsI) [41]		> 75 %	Prototype	Overall N_0 is still 3x smaller than expected
RD-26 - CERN [42]	-	> 85 % (2000 V)	Prototype	For higher wire gains θ starts being negative
RD-26 - Saclay [43]	-	> 78 %	Prototype	2 mm anode wire spacing would not operate in the test beam
RD-26 - Munich [44]	-	> 96 % (2600 V)	Prototype	A high efficiency obtained at a price if θ being negative
Princeton [45]	-	> 97 % (4100 V)	Prototype	A positive θ obtained with rather large anode-cathode spacing
Cornell prototype [46]		> 97 %	Prototype	Due to a very good noise performance a high efficiency obtained
CAPRICE [47]	> 90 %	> 60 %	Yes	The cathode efficiency will be improved in future balloon flights
RICH-II [48]	-	> 60 % (goal)	Prototype	Planned for the balloon flights
JETSET [49]	> 90 %	-	Yes	Advantage : TMAE based detector operating at ambient temp.
HERA-B (TMAE) [50]	> 90 %	-	Prototype	
College de France [51]			Prototype	TMAE-based prototype in preparation for 1995
HELIOS - pads [52]	-	> 95 %	Prototype	Prototype for CERES, except the HELIOS has the low pressure
PHENIX [53]	-	> 95 %	Prototype	Single gap parallel plate chamber at low pressure
HELIOS - optical [56]	-	> 90 % (optical)	Prototype	Deposit of N_{prim}~20 e$^-$ will cause a spark
NA35 - optical [57]	-	> 50-60 % (optical)	Prototype	Deposit of N_{prim}~20 e$^-$ will cause a spark; 1 spark / spill
Munich microstrip [58]	> 63 % (refl.mode)	> 6.5 % (refl.mode)	Prototype	Cathode pad efficiency small due to a small coupling to anode
Pisa microgap [59]	-	> 96 %	Prototype	A very large electric gradient across the anode-cathode gap
Weizmann microstrip [60]			Prototype	Semitransparent Q.E. is only ~10% at 170 nm.

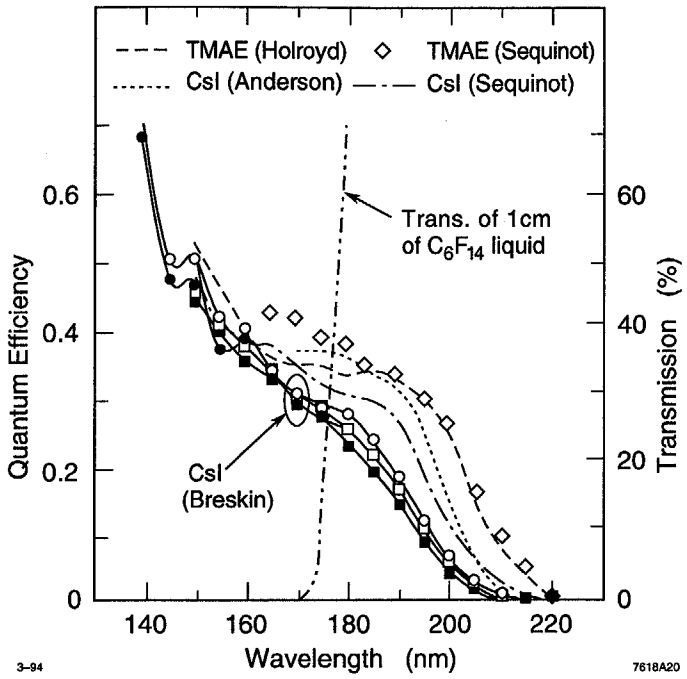
TMAE (Holroyd)
TMAE (Sequinot)
CsI (Anderson)
CsI (Sequinot)
Trans. of 1cm of C_6F_{14} liquid
CsI (Breskin)
Quantum Efficiency
Transmission (%)
Wavelength (nm)
0.6
0.4
0.2
0
60
40
20
0
140
160
180
200
220
3-94
7618A20

Fig. 1

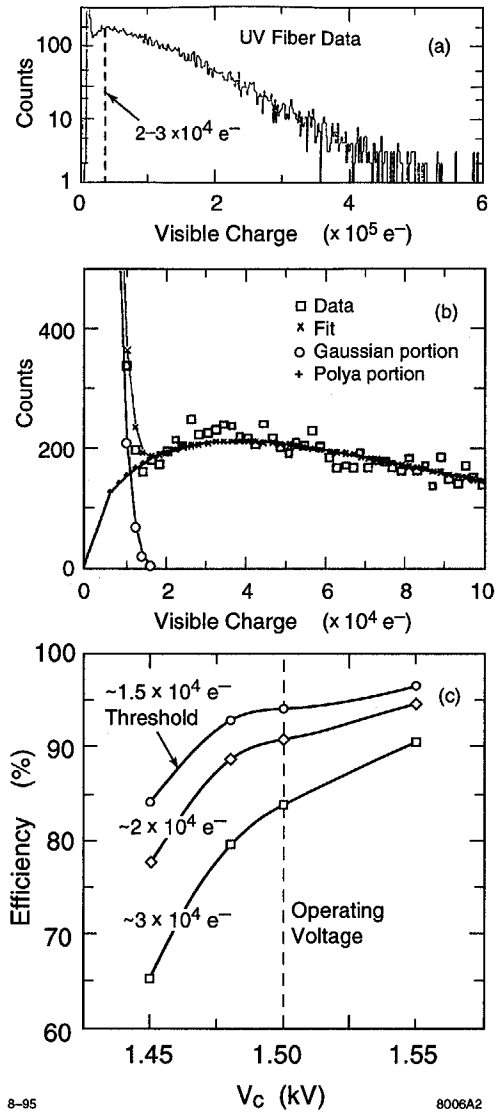
UV Fiber Data
(a)
Counts
100
10
1
2–3 x10^4 e$^-$
0
2
4
6
Visible Charge (x 10^5 e$^-$)
Data
Fit
Gaussian portion
Polya portion
(b)
Counts
400
200
0
0
2
4
6
8
10
Visible Charge (x 10^4 e$^-$)
100
~1.5 x 10^4 e$^-$
Threshold
(c)
~2 x 10^4 e$^-$
~3 x 10^4 e$^-$
Operating Voltage
Efficiency (%)
90
80
70
60
1.45
1.50
1.55
V_C (kV)
8-95
8006A2

Fig. 2

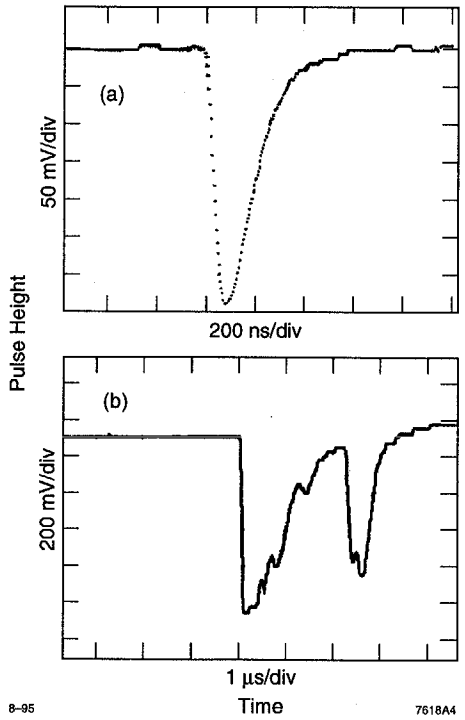
(a)
50 mV/div
200 ns/div
(b)
200 mV/div
1 µs/div
Time
Pulse Height
8-95
7618A4

Fig. 3

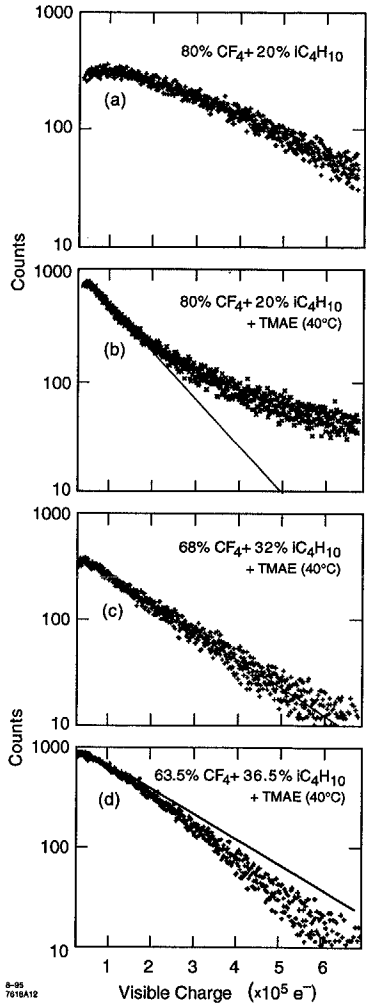
80% CF4+ 20% iC4H10
(a)
80% CF4+ 20% iC4H10
+ TMAE (40°C)
(b)
68% CF4+ 32% iC4H10
+ TMAE (40°C)
(c)
63.5% CF4+ 36.5% iC4H10
+ TMAE (40°C)
(d)
Counts
1000
100
10
1
2
3
4
5
6
Visible Charge (x10^5 e^-)
8-95
7618A12

Fig. 4

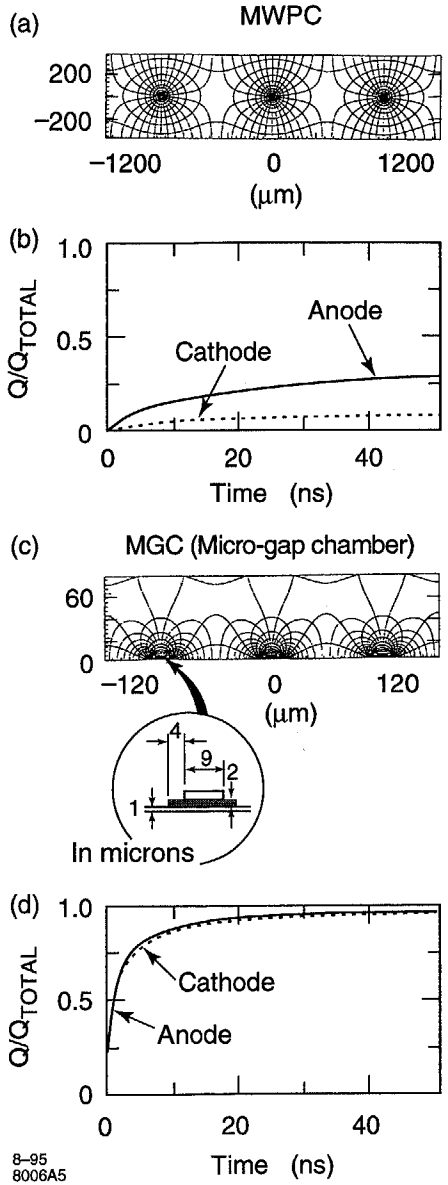
(a)
MWPC
200
−200
−1200
0
1200
(μm)
(b)
1.0
0.5
0
Q/Q_TOTAL
Anode
Cathode
0
20
40
Time (ns)
(c)
MGC (Micro-gap chamber)
60
0
−120
0
120
(μm)
4
9
2
1
In microns
(d)
1.0
0.5
0
Q/Q_TOTAL
Cathode
Anode
0
20
40
Time (ns)
8–95
8006A5

Fig. 5

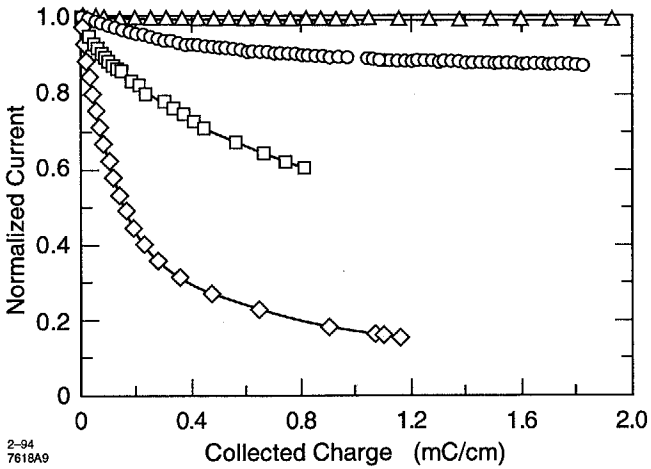
1.0
0.8
0.6
0.4
0.2
0
Normalized Current
0
0.4
0.8
1.2
1.6
2.0
Collected Charge (mC/cm)
2–94
7618A9

Fig. 6

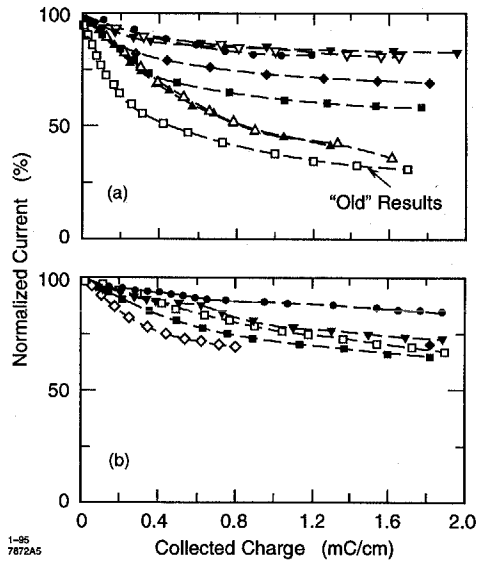
100
50
0
Normalized Current (%)
(a)
"Old" Results
100
50
0
(b)
0
0.4
0.8
1.2
1.6
2.0
Collected Charge (mC/cm)
1-95
7872A5

Fig. 7

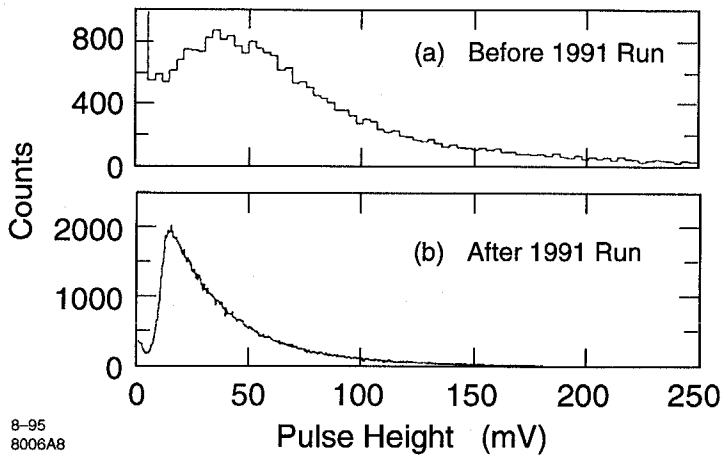
800
400
0
(a) Before 1991 Run
Counts
2000
1000
0
(b) After 1991 Run
0
50
100
150
200
250
Pulse Height (mV)
8-95
8006A8

Fig. 8

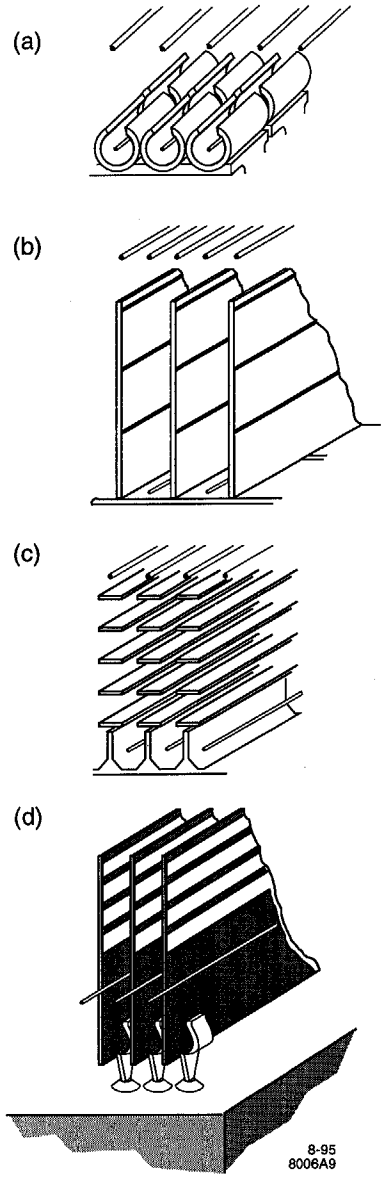
(a)
(b)
(c)
(d)
8-95
8006A9

Fig. 9

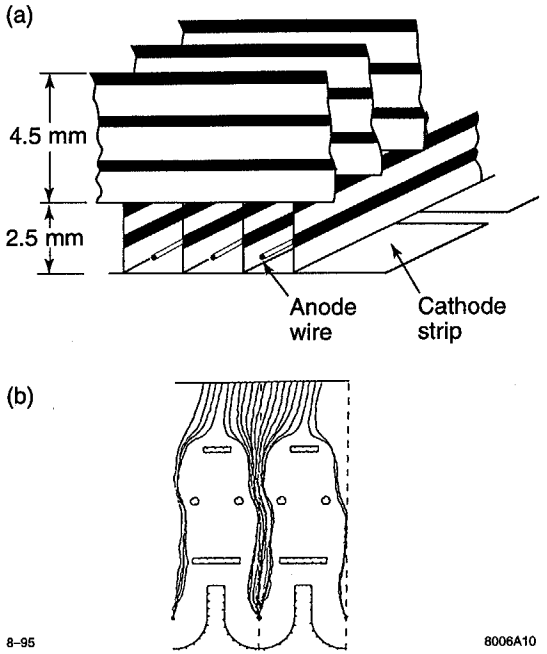
(a)
4.5 mm
2.5 mm
Anode wire
Cathode strip
(b)
8-95
8006A10

Fig. 10

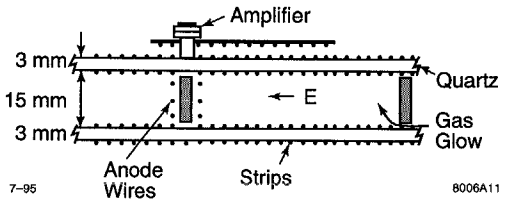
Amplifier
3 mm
15 mm
3 mm
Quartz
E
Gas
Glow
Anode
Wires
Strips
7–95
8006A11

Fig. 11

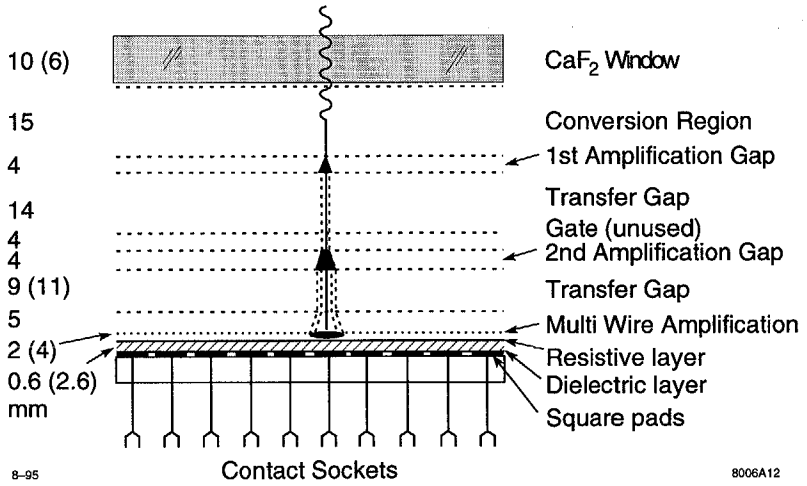
10 (6)
CaF2 Window
15
Conversion Region
4
1st Amplification Gap
14
Transfer Gap
4
Gate (unused)
4
2nd Amplification Gap
9 (11)
Transfer Gap
5
Multi Wire Amplification
2 (4)
Resistive layer
0.6 (2.6)
Dielectric layer
mm
Square pads
Contact Sockets
8–95
8006A12

Fig. 12

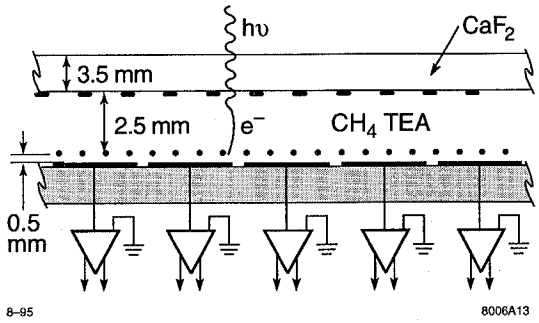
hυ
CaF2
3.5 mm
2.5 mm
e⁻
CH4 TEA
0.5 mm
8-95
8006A13

Fig. 13

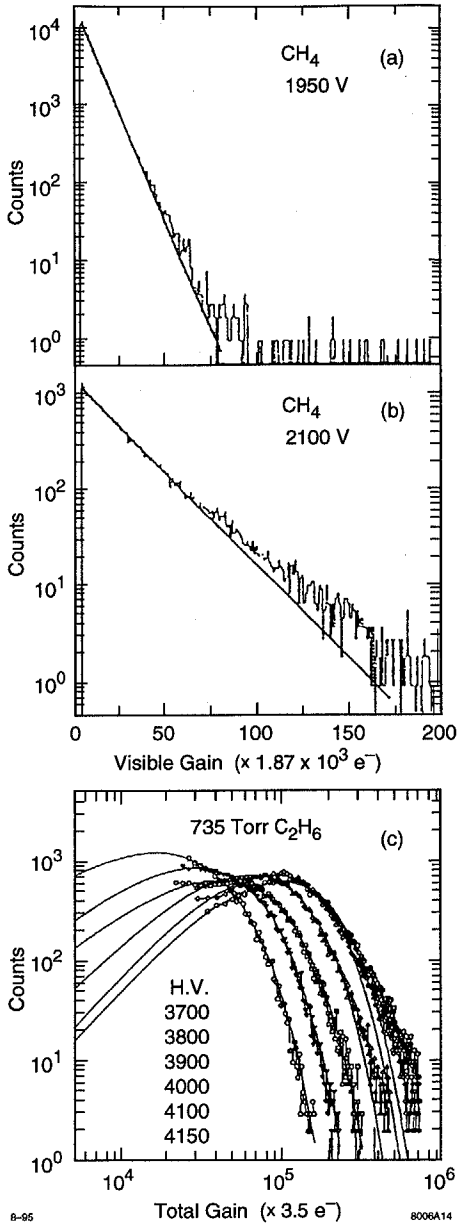
CH4
(a)
1950 V
Counts
CH4
(b)
2100 V
Counts
Visible Gain (x 1.87 x 10³ e⁻)
735 Torr C2H6
(c)
H.V.
3700
3800
3900
4000
4100
4150
Counts
Total Gain (x 3.5 e⁻)
8-95
8006A14

Fig. 14

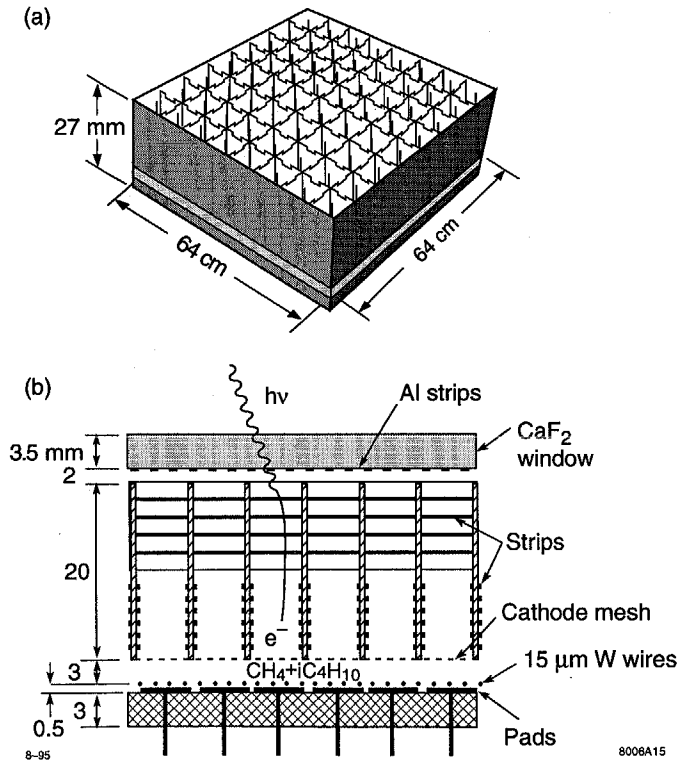
(a)
27 mm
64 cm
64 cm
(b)
hν
Al strips
CaF2 window
3.5 mm
2
20
Strips
Cathode mesh
e⁻
15 μm W wires
CH4+iC4H10
3
3
0.5
Pads
8-95
8006A15

Fig. 15

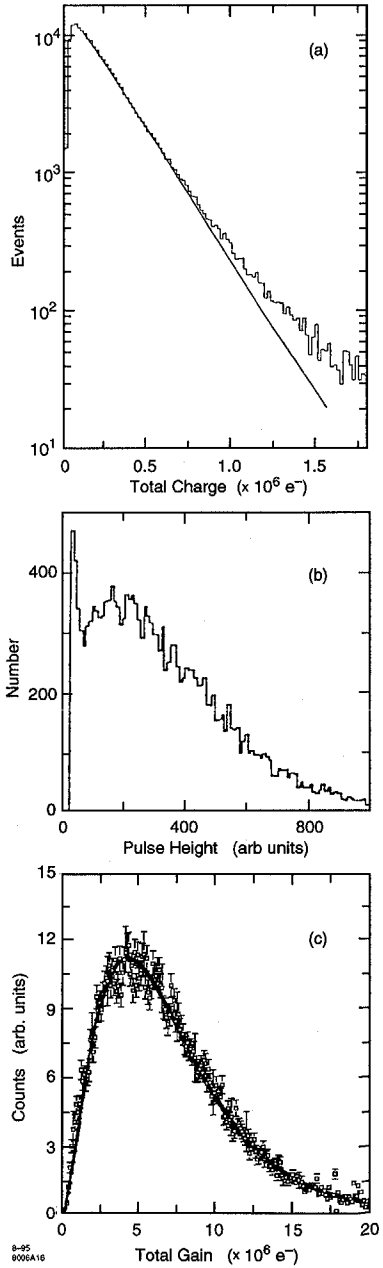
(a)
Events
Total Charge (x 10⁶ e⁻)
(b)
Number
Pulse Height (arb units)
(c)
Counts (arb. units)
Total Gain (x 10⁶ e⁻)
8-95
8006A16

Fig. 16

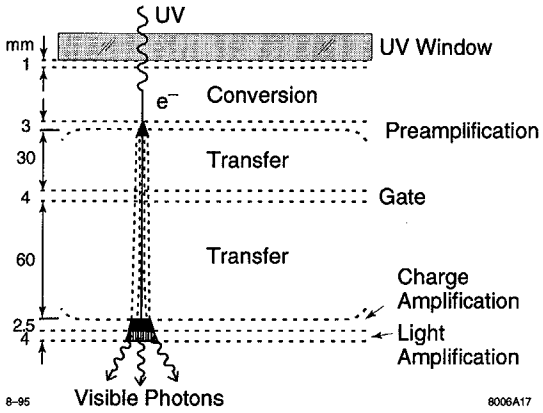
UV
mm
1
UV Window
e⁻
Conversion
3
Preamplification
30
Transfer
4
Gate
60
Transfer
Charge
Amplification
2,5
4
Light
Amplification
Visible Photons
8-95
8006A17

Fig. 17

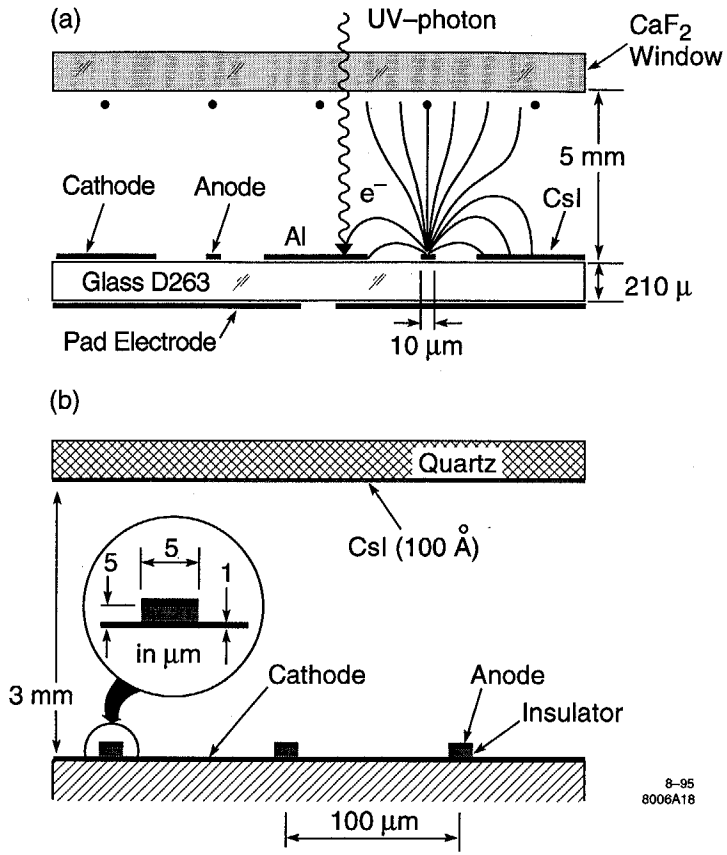
(a)
UV-photon
CaF2
Window
5 mm
Cathode
Anode
e⁻
CsI
Al
Glass D263
210 µ
Pad Electrode
10 µm
(b)
Quartz
CsI (100 Å)
5
5
1
in µm
3 mm
Cathode
Anode
Insulator
8-95
8006A18
100 µm

Fig. 18

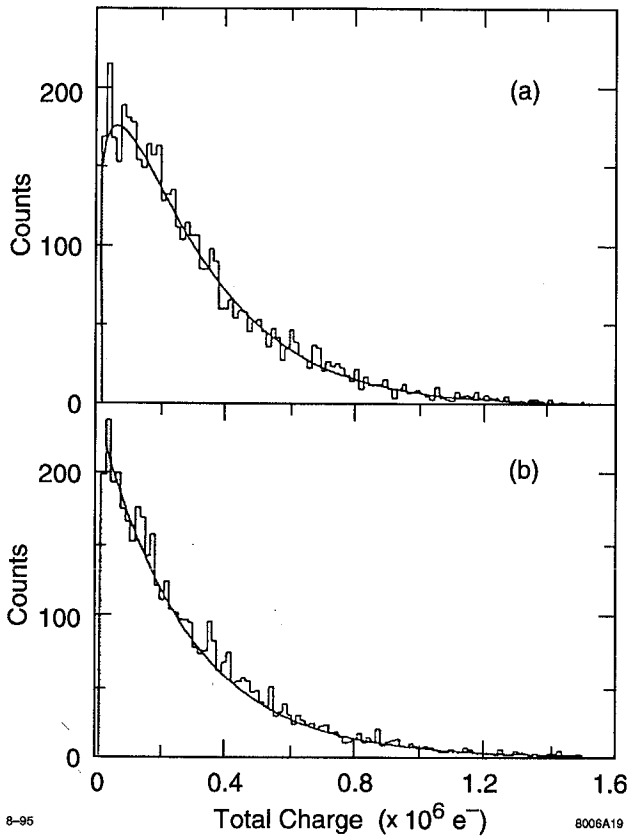
(a)
(b)
Counts
200
100
0
0
0.4
0.8
1.2
1.6
Total Charge (x 10^6 e^-)
8-95
8006A19

Fig. 19

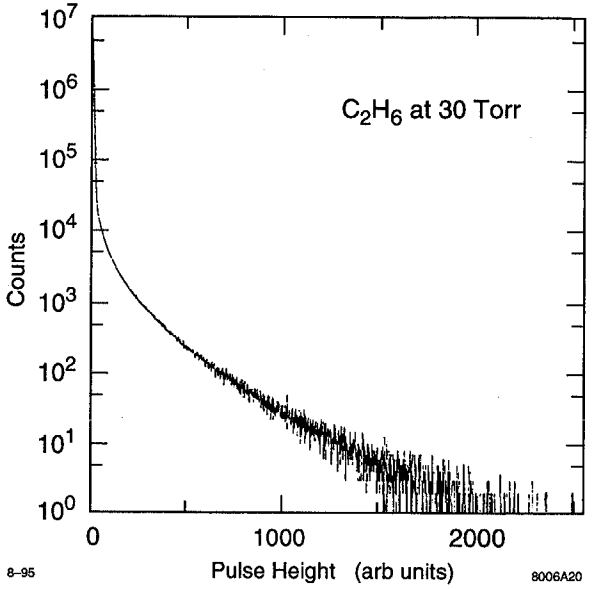
C2H6 at 30 Torr
Counts
10^7
10^6
10^5
10^4
10^3
10^2
10^1
10^0
0
1000
2000
Pulse Height (arb units)
8-95
8006A20

Fig.20

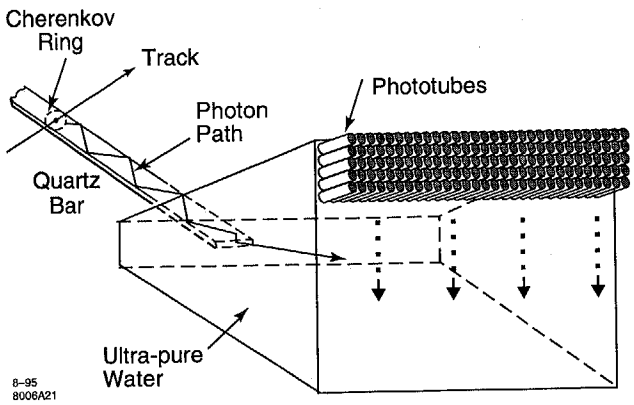
Cherenkov
Ring
Track
Photon
Path
Phototubes
Quartz
Bar
Ultra-pure
Water
8-95
8006A21

Fig. 21

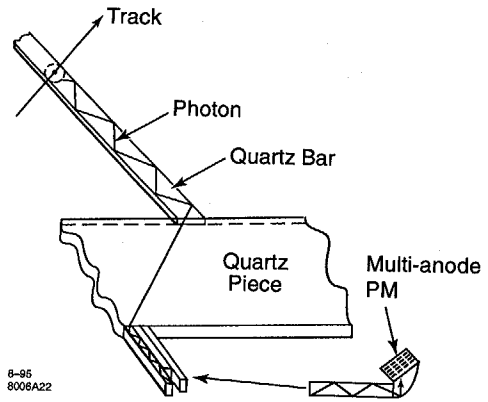
Track
Photon
Quartz Bar
Quartz
Piece
Multi-anode
PM
8-95
8006A22

Fig. 22

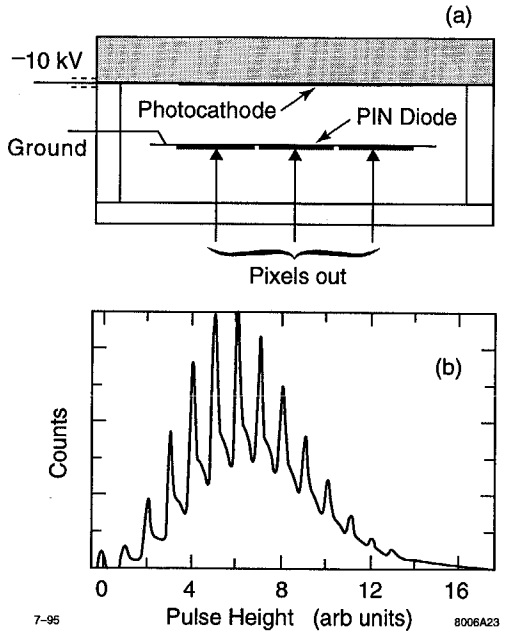
(a)
−10 kV
Photocathode
PIN Diode
Ground
Pixels out
(b)
Counts
0
4
8
12
16
Pulse Height (arb units)
7-95
8006A23

Fig. 23

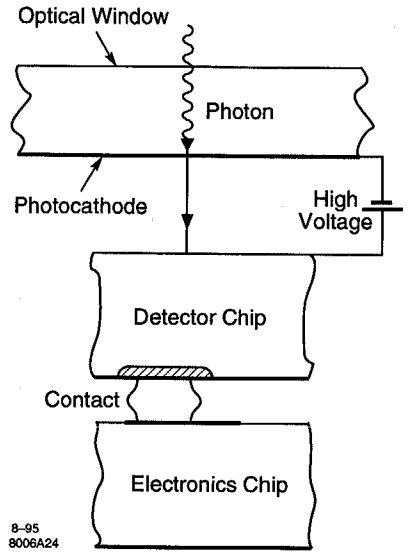
Optical Window
Photon
Photocathode
High Voltage
Detector Chip
Contact
Electronics Chip
8-95
8006A24

Fig. 24

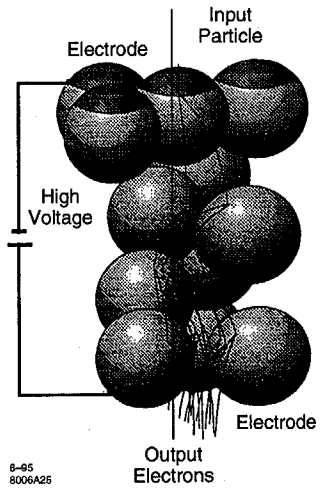
Input
Particle
Electrode
High
Voltage
Electrode
Output
Electrons
6-95
8006A25

Fig. 25